Construction and analysis of a HDG solution for the total-flux-formulation of the convected Helmholtz equation

Hélène Barucq, Nathan Rouxelin, Sébastien Tordeux

CONSTRUCTION AND ANALYSIS OF A HDG SOLUTION FOR THE TOTAL-FLUX FORMULATION OF THE CONVECTED HELMHOLTZ EQUATION

HÉLÈNE BARUCQ, NATHAN ROUXELIN, AND SÉBASTIEN TORDEUX

Abstract. We introduce a HDG method for the convected Helmholtz equation based on the total flux formulation, in which the vector unknown represents both diffusive and convective phenomena. This HDG method is constricted with the same interpolation degree for all the unknowns and a physically informed value for the penalization parameter is computed. A detailed analysis including local and global well-posedness, as well as a superconvergence result is carried out. We then provide numerical experiments to illustrate the theoretical results.

Introduction

Aeroacoustic waves are widely studied because they are at the core of many applications in everyday life. We can mention the aeronautics, the automobile with for example all the studies aiming at the reduction of the noise whose nuisance is not anymore to show. Less standard are the numerical simulations used to understand the interior of non-probeable environments such as stars and among them, the closest to our planet, namely the sun. Here again, aeroacoustic waves play a key role as depicted in [GBD+17, Chr04] where they are used to describe solar oscillations which can be measured on the surface of the sun. We are thus interested in developing an advanced computational environment to numerically probe the interior of the Sun. This work is a first step in the development of an advanced computational environment to probe numerically the interior of the sun. Behind this idea is the need to solve inverse problems and in this perspective, we want to use the code `hawen` ([Fau21]) which proposes an optimized environment to perform Full Waveform Inversion with wave equations posed in harmonic regime. With `hawen`, it has been shown that formulations based on discontinuous finite elements are particularly well suited (see for example [FS20] for the case of acoustic seismic waves) to the extent that a hybridized formulation is used. Indeed, it is absolutely necessary to reduce the size of the linear system to be solved if one wants to consider large scale applications such as the reconstruction of the interior of the sun. In this paper, we consider the so-called *Hybridizable Discontinuous Galerkin Methods* (HDG), which relies on a static condensation process of a DG formulation leading to express the discrete problem in terms of the solution of a global problem set on the mesh skeleton. The volume unknowns are next computed thanks to the solution of small local problems defined element-wise and in parallel.

1991 *Mathematics Subject Classification.* Primary 65N12, 65N30.

Key words and phrases. Hybridizable Discontinuous Galerkin Method (HDG), aeroacoustics, convected Helmholtz equation, harmonic regime, error estimates.

Nathan Rouxelin is supported by a grant from e2s-UPPA..

HDG have been considered by numerous authors for various problems such as elliptic equations in [CGL09, CDG+09, CC12, CC14], acoustic wave propagation in [GM11, GSV18, NPRC15], elastic wave propagation in [HPS17, BDMP21, CS13, FCS15, BCDL15] and, Maxwell equations in [CQSS17, CQS18, CLOS20]. Very recently, these methods have also been used to implement quantitative inverse problems in [FS20] where a specific formulation of the adjoint method is developed.

Theory for HDGs is rather similar to the one for mixed finite elements and the actual connection was first established by Cockburn and his coworkers in [CGS10]. For a self-contained introduction to the theory of HDG, we refer to [DS19] while a historical perspective on HDG can be found in [Coc14].

A comparison between HDG and Continuous Galerkin methods has been carried out in [KSC12, YMKS16] for two-dimensional elliptic diffusion problems. The authors have shown that it is possible to implement a high-order HDG method with the same accuracy and cost as a continuous finite element method. This is a very important result for some applications where it is preferable to use a discontinuous finite element method to benefit for example from the *hp*-adaptivity ([Jac21]) or to guarantee a higher resistance to numerical dispersion ([BBF+17]). As far as face-based finite element methods are concerned, Hybrid High-Order (HHO) methods can also be considered and it was shown in [CDPE16] that regarding the linear elasticity, this method could be interpreted as an HDG method after rewriting it in a mixed formulation. To our knowledge, this study has not been done for Helmholtz problems. However, very recently, it has been shown in [BDE21] that the HHO method can be very useful to solve the single continuation problem subject to the Helmholtz equation.

In this paper, we construct a HDG method based on the *total flux formulation* of the convected Helmholtz equation. This formulation is well-suited for HPC and leads to accurate numerical results as it is super-convergent. This method can also be constructed as the hybridized version of a upwind DG method, leading to a physically informed choice of penalization parameters. The implementation of the method does not depend on the choice of such in general arbitrary parameters that might perturb the accuracy of the numerical solution if badly chosen. The content of this work is organized as follows. Section 1 is dedicated to the convected Helmholtz equation and the total flux formulation, which is the first-order in space formulation used to construct the HDG method of this paper. Section 2 deals with the approximation setting including discrete spaces. In Section 3, we derive a hybridized DG method for the convected Helmholtz equation. In Section 4, we construct a physically-informed choice of penalization parameter based on the equivalence between the HDG formulation of the previous section and an upwind DG method. In Section 5: we study the well-posedness of the local problems of the HDG method. In Section 6: we study the convergence rate of the method. In Section 7: we study the well-posedness of the global problem of the HDG method. In Section 8: we present numerical experiments to illustrate our theoretical results.

1. Model problem

As a model problem we consider the so-called *convected Helmholtz equation*

$$\rho_0 \left(-\omega^2 p - 2i\omega \boldsymbol{v_0} \cdot \nabla p + \boldsymbol{v_0} \cdot \nabla(\boldsymbol{v_0} \cdot \nabla p)\right) - \operatorname{div}\left(\rho_0 c_0^2 \nabla p\right) = s \tag{1}$$

where ω is the angular frequency, ρ_0 is the density of the fluid, $\boldsymbol{v_0}$ is the velocity of the fluid, c_0 is the adiabatic sound speed, and s is the acoustic source.
Equation (1) is the simplest aeroacoustic model and therefore has a limited validity. This equation can be used for

- a *uniform background flow*, in this case the unknown p can be interpreted as a pressure perturbation,
- a *potential background flow*, in this case the unknown p should be interpreted as an *acoustic potential* and the physical quantities can be retrieved using the following identities

$$\begin{aligned} &\text{Pressure perturbation:} && p' = -\rho_0 c_0(-i\omega + \boldsymbol{v_0}\cdot\nabla)p, \\ &\text{Velocity perturbation:} && \boldsymbol{v}' = -c_0\nabla p, \end{aligned}$$

see [Pie90, Sec. II.].
In this paper, we only consider finite computational domains, which we denote by $\mathcal{O}$ and whose boundary is denoted by Γ. More precisely $\mathcal{O}$ is a bounded open subset of $\mathbb{R}^n$ with $n = 2$ or 3. We will assume that the background flow is incompressible which leads to the following local mass conservation equation

$$\operatorname{div}(\rho_0 \boldsymbol{v_0}) = 0. \tag{2}$$

Furthermore, we require some additional regularity for the velocity field $\rho_0\boldsymbol{v_0}$ assuming that it is *Lipschitz continuous*, *i.e.* $\rho_0\boldsymbol{v_0} \in \boldsymbol{W}^{1,\infty}(\mathcal{O})$. This will be useful to derive convergence estimates for the method as it allows us to estimate the difference between $\rho_0\boldsymbol{v_0}$ and its average on a mesh element.
To get a mixed Discontinuous Galerkin approximation of the convected Helmholtz equation, we rewrite (3) as a system involving only first-order in space derivatives. We first combine the Laplace operator and the second-order convection term to obtain an anisotropic Laplace operator, which can be naturally handled in a HDG formulation. Using the mass conservation assumption (2), we have

$$\rho_0\boldsymbol{v_0}\cdot\nabla(\boldsymbol{v_0}\cdot\nabla p) = \operatorname{div}\left(\rho_0\boldsymbol{v_0}\boldsymbol{v_0}^T\nabla p\right).$$

Introducing the anisotropy tensor $\boldsymbol{K_0} := \rho_0\left(c_0^2\mathbf{Id} - \boldsymbol{v_0}\boldsymbol{v_0}^T\right)$, we obtain

$$\rho_0\left(-\omega^2 p - 2i\omega\boldsymbol{v_0}\cdot\nabla p\right) - \operatorname{div}\left(\boldsymbol{K_0}\nabla p\right) = s. \tag{3}$$

To lighten the notations in the remaining of this paper, we introduce the following vector field

$$\boldsymbol{b_0} := \rho_0\boldsymbol{v_0},$$

that satisfies the following mass conservation equation

$$\operatorname{div}(\boldsymbol{b_0}) = 0.$$

We notice that

$$2i\omega\boldsymbol{b_0}\cdot\nabla p = \operatorname{div}\left(2i\omega p\boldsymbol{b_0}\right),$$

and we can therefore rewrite (3) as

$$-\rho_0\omega^2 p - \operatorname{div}\left(\boldsymbol{K_0}\nabla p + 2i\omega p\boldsymbol{b_0}\right) = s. \tag{4}$$

If the background flow is subsonic, i.e.

$$\inf_{\mathcal{O}}\left(c_0^2 - |\boldsymbol{v_0}|^2\right) > 0, \tag{5}$$

then we have the following lemma.

Lemma 1.1. *The anisotropy tensor $\boldsymbol{K_0}$ is symmetric positive-definite and its spectrum is*

$$\mathrm{Sp}(\boldsymbol{K_0}) = \left\{\rho_0 c_0^2, \rho_0(c_0^2 - |\boldsymbol{v_0}|^2)\right\}$$

Proof: We have $\boldsymbol{K_0 v_0} = \rho_0 \left(c_0^2 - |\boldsymbol{v_0}|^2\right) \boldsymbol{v_0}$ and $\boldsymbol{K_0 u} = \rho_0 c_0^2 \boldsymbol{u}$ for all $\boldsymbol{u} \in \boldsymbol{v_0}^\perp$.

We can conclude that $-\mathrm{div}\left(\boldsymbol{K_0}\nabla p\right)$ is an elliptic operator.
To obtain a well-posed problem, the equation (4) must be closed by adding some boundary conditions on Γ. In this paper, we only consider Neumann boundary conditions

$$(\boldsymbol{K_0}\nabla p + 2i\omega p \boldsymbol{b_0}) \cdot \boldsymbol{n} = g_N, \quad \text{on } \Gamma, \tag{6}$$

where $\boldsymbol{n}$ is the outward-facing unitary normal vector to Γ. In this case, the bilinear form associated with the convected Helmholtz equation has a *coercive + compact* structure and is therefore of Fredholm type. This implies that the system (4)–(6) has a unique solution, except for some frequencies ω for which a resonant phenomenon can occur. In this paper, we will always assume that ω is not a resonant frequency.

To construct a HDG formulation, we need to rewrite (4) as a first-order in space system. It is therefore natural to introduce the *total flux*

$$\boldsymbol{\sigma} := -\boldsymbol{K_0}\nabla p - 2i\omega p \boldsymbol{b_0}.$$

The resulting first-order formulation for (4) supplemented with the Neumann condition (6) reads

$$\boldsymbol{W_0}\boldsymbol{\sigma} + \nabla p + 2i\omega p \boldsymbol{W_0 b_0} = 0, \qquad \text{in } \mathcal{O}, \tag{7a}$$

$$-\rho_0\omega^2 p + \mathrm{div}\left(\boldsymbol{\sigma}\right) = s, \qquad \text{in } \mathcal{O}, \tag{7b}$$

$$\boldsymbol{\sigma} \cdot \boldsymbol{n} = -g_N, \qquad \text{on } \Gamma, \tag{7c}$$

where $\boldsymbol{W_0}$ is the inverse of $\boldsymbol{K_0}$. Note that $\boldsymbol{K_0}$ is always invertible as

$$\det \boldsymbol{K_0} = \rho_0 c_0^2 \left(c_0^2 - |\boldsymbol{v_0}|^2\right) \neq 0,$$

and its inverse can be expressed as

$$\boldsymbol{W_0} := \boldsymbol{K_0}^{-1} = \frac{1}{\rho_0 c_0^2}\left[\mathbf{Id} + \frac{\boldsymbol{v_0}\boldsymbol{v_0}^T}{c_0^2 - |\boldsymbol{v_0}|^2}\right].$$

thanks to the *Sherman-Morrison formula* [SM50].
Notice that even if we have chosen to work with second-order in frequency reading (7a)–(7b)–(7c), the resulting method can easily be adapted to obtain a first-order in frequency one. Indeed, the following system can be obtained

$$-i\omega\boldsymbol{W_0}\boldsymbol{\sigma} + \nabla p + 2i\omega p \boldsymbol{W_0 b_0} = 0,$$
$$-i\omega p + \mathrm{div}\left(\boldsymbol{\sigma}\right) = s,$$

instead of (7a)–(7b).

2. Approximation settings

In this section, we introduce the notations and approximation spaces that will be used to construct the HDG method considered in this paper.

2.1. **Approximation spaces.** We consider a mesh $\mathcal{T}_h$ of the domain $\mathcal{O}$. For a given element $K \in \mathcal{T}_h$ we denote its diameter by h_K and we set

$$h := \max_{K\in\mathcal{T}_h} h_K.$$

For an element $K \in \mathcal{T}_h$, we denote by $\mathcal{E}(K)$ the set of its edges. We also consider

- The set of all edges of $\mathcal{T}_h$:

$$\mathcal{E}_h := \bigcup_{K\in\mathcal{T}_h} \mathcal{E}(K).$$

- The set of boundary edges:

$$\mathcal{E}_h^b := \{e \in \mathcal{E}_h \mid e \subset \Gamma\}.$$

- The set of interior edges:

$$\mathcal{E}_h^i := \{e \in \mathcal{E}_h \mid \exists K_+, K_- \in \mathcal{T}_h,\ K_- \neq K_+,\ e = \partial K_+ \cap \partial K_-\}.$$

Remark 2.1: We will assume that the mesh $\mathcal{T}_h$ has the usual *shape-regularity* property, see [EG04, Def. 1.107].

For $K \in \mathcal{T}_h$, we denote by $\mathcal{P}_k(K)$ the space of polynomial functions of total degree at most k defined on K. We will also use the space of vectorial polynomials $\boldsymbol{\mathcal{P}}_k(K) = \mathcal{P}_k(K)^n$. Even if those spaces can be defined for $k > 0$, in this paper we will usually assume that $k > 2$ as HDG methods of lower order have limited interest from a computational point of view. Indeed the key step in HDG methods is a static condensation process which consists in eliminating the interior degrees of freedom. The later do not exist for polynomial approximation of degree 1 or 2. Furthermore it was noted in [KSC12] that HDG method have a cost similar to CG methods for polynomial approximation of degree 5 or higher. However the static condensation of lower-order HDG methods has one practical interest: it leads to a mixed DG method which has the same cost as a primal DG method.

On each element $K \in \mathcal{T}_h$, we introduce the following approximation spaces for the pressure and the flux

$$\begin{aligned} \boldsymbol{V}_h(K) &:= \boldsymbol{\mathcal{P}}_k(K) \quad && \text{for the flux } \boldsymbol{\sigma}_h, \\ W_h(K) &:= \mathcal{P}_k(K) && \text{for the potential } p_h. \end{aligned}$$

As the approximation spaces are discontinuous, we introduce the numerical fluxes $\widehat{\boldsymbol{\sigma}_h}$ and $\widehat{p_h}$ which are designed to approximate the traces of $\boldsymbol{\sigma}$ and p on the boundary of the elements. Those numerical fluxes also include some stabilization terms that ensure the stability of the DG method. In the particular case of HDG methods, a *static condensation* process is used to express $\boldsymbol{\sigma}_h$, p_h and $\widehat{\boldsymbol{\sigma}_h}$ as a function of $\widehat{p_h}$. This leads to a so-called *global problem* whose unknown is the numerical flux $\widehat{p_h}$. To approximate $\widehat{p_h}$ we introduce the following space for $e \in \mathcal{E}(K)$

$$M_h(e) := \mathcal{P}_k(e).$$

As those approximation spaces are discontinuous, we can construct the *global approximation spaces* from the local ones

$$\begin{aligned} \boldsymbol{V}_h &:= \left\{\boldsymbol{\sigma} \in \boldsymbol{L}^2(\mathcal{O}) \;\middle|\; \boldsymbol{\sigma}|_K \in \boldsymbol{V}_h(K), \forall K \in \mathcal{T}_h\right\} && \text{for the flux } \boldsymbol{\sigma}_h, \\ W_h &:= \left\{p \in L^2(\mathcal{O}) \;\middle|\; p|_K \in W_h(K), \forall K \in \mathcal{T}_h\right\} && \text{for the potential } p_h, \\ M_h &:= \left\{\mu \in L^2(\mathcal{E}_h) \;\middle|\; \mu|_e \in M_h(e), \forall e \in \mathcal{E}_h\right\} && \text{for the trace } \widehat{p_h}. \end{aligned}$$

In FIGURE 1, we have depicted the differences in the *degrees of freedom* for the continuous (CG), discontinuous (DG) and hybridizable discontinuous (HDG) Galerkin methods. The degrees of freedom of the HDG methods are the ones associated with the numerical trace $\widehat{p_h}$. If a mixed DG method is used, there are three unknowns for each degree of freedom, thus rendering those methods even more expensive. It was demonstrated in [KSC12] that HDG methods have numerical cost similar to the one of CG methods when they are properly implemented. Despite being expensive from a computational point of view, DG methods have been known to have some attratctive properties. In particular, they can naturally be implemented for a arbitrary high-order with *hp*-adaptativity and in a parallel way. Using HDG methods therefore allows to keep those advantages of the DG methods for a reduced numerical cost, as it is illustrated in FIGURE 2. As the numerical cost of the method is directly linked to the number of degrees of freedom, we can clearly see that the HDG method is less expensive than the DG method.

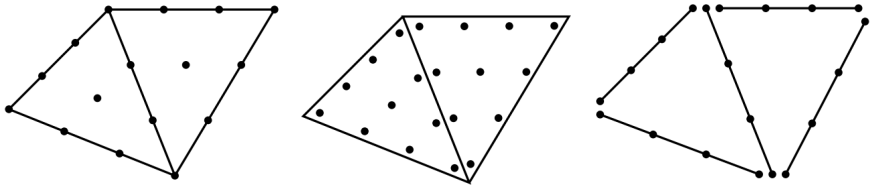

(A) CG (B) DG (C) HDG

FIGURE 1. Polynomial interpolation of degree 3

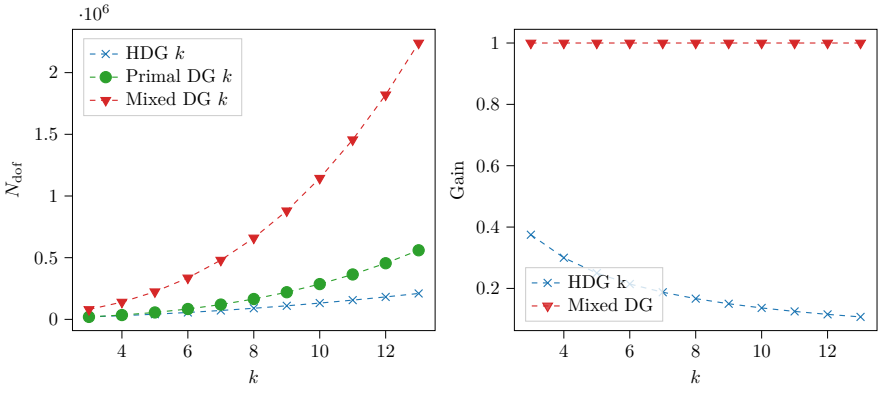

(A) Number of degrees of freedom (B) Gain with respect to mixed DG

FIGURE 2. Number of degrees of freedom for a mixed DG method, a primal DG method (based on the second-order formulation) and a HDG method with interpolation degree k in 3D with 10^3 elements.

Remark 2.2: It is also possible to choose a continuous space for $\widehat{p_h}$, this leads to the so-called *Locally Discontinuous but Globally Continuous method* (LDGC), see *eg.* [ALA13, FLd14]. However this choice does not seem to improve the convergence rate of the method.

2.2. **Hermitian products and norms.** The complex conjugate of z is denoted by $\overline{z}$. For an element $K \in \mathcal{T}_h$, we denote the L^2-inner product[1] and its associated norm by

$$(u,v)_K := \int_K u \cdot \overline{v} \mathrm{d}\boldsymbol{x} \quad \text{and} \quad \|u\|_K^2 := (u,u)_K .$$

We then introduce the broken inner product

$$(u,v)_{\mathcal{T}_h} := \sum_{K\in\mathcal{T}_h} (u,v)_K ,$$

and we denote by $\|\cdot\|_{\mathcal{T}_h}$ the associated norm. On the boundary of an element K, we also introduce the local inner product

$$\langle u,v\rangle_{\partial K} := \sum_{e\in\mathcal{E}(K)} \int_e u \cdot \overline{v} \mathrm{d}\sigma,$$

and the associated norm is denoted by $\|\cdot\|_{\partial K}$. The broken inner product is then defined as

$$\langle u,v\rangle_{\partial\mathcal{T}_h} := \sum_{K\in\mathcal{T}_h} \sum_{e\in\mathcal{E}(K)} \langle u|_K, v|_K\rangle_e ,$$

and we denote by $\|\cdot\|_{\partial\mathcal{T}_h}$ the associated norm. Here we would like to point out that, depending on the regularity of u and v, $\langle\cdot,\cdot\rangle_{\partial K}$ can denote either the inner product of $L^2(\partial K)$ or the duality bracket between $H^{-\frac{1}{2}}(\partial K)$ and $H^{\frac{1}{2}}(\partial K)$. It is worth noting that the quantity $\langle\cdot,\cdot\rangle_{\partial\mathcal{T}_h}$ is dual valued on the interior edges. We will sometimes need to work on the interior edges only and we define the following broken product

$$\langle u,v\rangle_{\partial\mathcal{T}_h\setminus\Gamma} := \sum_{K\in\mathcal{T}_h} \sum_{e\in\mathcal{E}(K)\cap\mathcal{E}_h^i} \langle u|_K, v|_K\rangle_e .$$

Finally, we also introduce the following weighted norms

$$\|u\|_{\rho_0,K}^2 := (\rho_0 u, u)_K \qquad \text{which satisfies} \quad \|u\|_{\rho_0,K} \leqslant \|\rho_0\|_{L^\infty(K)}^{\frac{1}{2}} \|u\|_K$$
$$\|\boldsymbol{q}\|_{\boldsymbol{W_0},K}^2 := (\boldsymbol{W_0 q}, \boldsymbol{q})_K \qquad \text{which satisfies} \quad \|\boldsymbol{q}\|_{\boldsymbol{W_0},K} \leqslant C_{\boldsymbol{W_0},K} \|\boldsymbol{q}\|_K$$

where

$$C_{\boldsymbol{W_0},K} = \left(\max_K \frac{1}{\rho_0 \left(c_0^2 - |\boldsymbol{v_0}|^2\right)} \right)^{\frac{1}{2}}$$

is the largest eigenvalue of $\boldsymbol{W_0}$ in K, we recall that the spectrum of $\boldsymbol{K_0}$ (and therefore of $\boldsymbol{W_0} := \boldsymbol{K_0}^{-1}$) was given in Lemma 1.1.

[1]For vector fields, the $\mathbb{R}^n$ dot-product is used inside the integral as the conjugate is already applied.

2.3. **Edges, jumps and averages.** Discontinuity at the interface between elements distinguish DG formulations from the CG ones. For stability and implementation purposes, it is then required to define quantities related to the edges of the elements.
For an interior face $\mathcal{E}_h^i \ni e = \partial K_+ \cap \partial K_-$, we denote by $\boldsymbol{n}^+$ (resp. $\boldsymbol{n}^-$) the unitary outgoing normal vector of ∂K_+ (resp. ∂K_-). We will always assume that the flow $\boldsymbol{v_0}$ goes from K_- to K_+, as depicted on FIGURE 3.

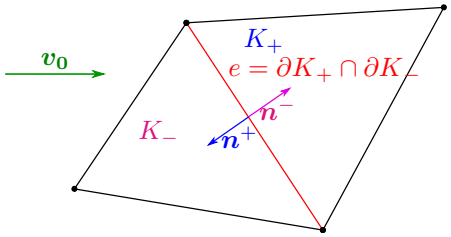

FIGURE 3. Normal vectors on an interior face

If e is a boundary edge, then $\boldsymbol{n}$ denotes the unitary normal vector outwardly directed to $\mathcal{O}$.
We will often use the *average operator* defined on the interior and boundary faces by

$$\begin{aligned} &\text{On } \mathcal{E}_h^i \ni e = \partial K_+ \cap \partial K_-, && \{\!\{\varphi\}\!\}_e := \frac{1}{2}\left(\varphi^+ + \varphi^-\right), \\ &\text{On } \mathcal{E}_h^b \ni e = \partial K \cap \Gamma, && \{\!\{\varphi\}\!\}_e := \frac{1}{2}\varphi, \end{aligned}$$

where φ can either be a scalar or vectorial quantity. We will also make frequent use of the *jump operator* defined on the interior and boundary faces by

$$\begin{aligned} &\text{On } \mathcal{E}_h^i \ni e = \partial K_+ \cap \partial K_-, && [\![\boldsymbol{q}]\!]_e := \boldsymbol{q}^+ \cdot \boldsymbol{n}^+ + \boldsymbol{q}^- \cdot \boldsymbol{n}^-, \\ &\text{On } \mathcal{E}_h^b \ni e = \partial K \cap \Gamma, && [\![\boldsymbol{q}]\!]_e := \boldsymbol{q} \cdot \boldsymbol{n}, \end{aligned}$$

for a vectorial quantity. Notice that with this definition, the jump operator only controls the normal part of the vector. For a scalar quantity, the *jump operator* is defined on the interior and boundary faces by

$$\begin{aligned} &\text{On } \mathcal{E}_h^i \ni e = \partial K_+ \cap \partial K_-, && [\![p]\!]_e := p^+\boldsymbol{n}^+ + p^-\boldsymbol{n}^-, \\ &\text{On } \mathcal{E}_h^b \ni e = \partial K \cap \Gamma, && [\![p]\!]_e := p\boldsymbol{n}, \end{aligned}$$

for a scalar quantity. A sketch of those quantities is given in FIGURE 4.

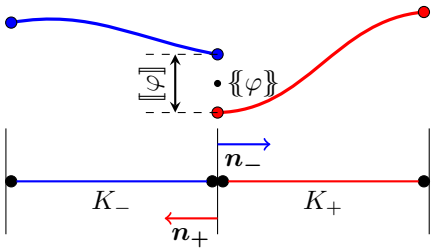

FIGURE 4. 1D-sketch of the jump and average on an interior node

3. Construction of the hybridized formulation

In this section, we construct the hybridized formulation for the upwind DG method of the previous section. This construction relies on the existence of an affine relationship between $\widehat{\boldsymbol{\sigma}_h}$ and $\widehat{p_h}$ which enables the parametrization of the volumetric unknowns $(\boldsymbol{\sigma}_h, p_h)$ only by $\widehat{p_h}$. Those volumetric unknown can then be eliminated thanks to a *static condensation* process leading to a *global problem* for $\widehat{p_h}$ only. This global problem encodes the continuity requirements of the solution between two elements as well as the boundary conditions of the problem. The original unknowns can then be recovered by independently solving a *local problem* on each element of the mesh.

3.1. **Local problem.** We write a DG variational formulation of (7a)–(7b) on an element $K \in \mathcal{T}_h$ leading to the *local problem* : seek $(\boldsymbol{\sigma}_h, p_h) \in \boldsymbol{V}_h(K) \times W_h(K)$ such that

$$(\boldsymbol{W_0}\boldsymbol{\sigma}_h, \boldsymbol{r}_h)_K - (p_h, \operatorname{div}(\boldsymbol{r}_h))_K + 2i\omega\,(p_h \boldsymbol{W_0}\boldsymbol{b_0}, \boldsymbol{r}_h)_K = -\langle \widehat{p_h}, \boldsymbol{r}_h \cdot \boldsymbol{n}\rangle_{\partial K}\,, \tag{8a}$$

$$-\omega^2\,(\rho_0 p_h, w_h)_K - (\boldsymbol{\sigma}_h, \nabla w_h)_K + \langle \widehat{\boldsymbol{\sigma}_h} \cdot \boldsymbol{n}, w_h\rangle_{\partial K} = (s, w_h)_K\,, \tag{8b}$$

for all $(\boldsymbol{r}_h, w_h) \in \boldsymbol{V}_h(K) \times W_h(K)$. In (8a)–(8b), the flux for p, denoted by $\widehat{p_h}$, is called the *numerical trace* and is now considered as an unknown of the problem. The next section will be devoted to the choice of flux for $\boldsymbol{\sigma}$.

3.2. **Transmission condition.** Due to the discontinuous nature of the approximation spaces, we need to link all the local problems together. To this end, we introduce the *numerical flux* for $\boldsymbol{\sigma}_h$

$$\widehat{\boldsymbol{\sigma}_h} \cdot \boldsymbol{n} := \boldsymbol{\sigma}_h \cdot \boldsymbol{n} + i\omega\tau(p_h - \widehat{p_h}), \tag{9}$$

which satisfies the following *transmission condition*

$$\langle \widehat{\boldsymbol{\sigma}_h} \cdot \boldsymbol{n}, \mu_h\rangle_{\partial\mathcal{T}_h} = \langle g_N, \mu_h\rangle_{\Gamma} \tag{10}$$

for all $\mu_h \in M_h$, and using the value of τ derived in Proposition 4.3 of Section 4. We recall that functions in M_h are piecewise polynomials that are only discontinuous at the geometric nodes. Notice that (10) enforces the normal continuity of $\widehat{\boldsymbol{\sigma}_h}$ on the interior faces as well as the Neumann boundary conditions on Γ.
We recall that on an interior edge $\mathcal{E}_h^i \ni e = \partial K_+ \cap \partial K_-$, the jump operator is defined as

$$[\![\boldsymbol{\sigma}_h]\!] := \boldsymbol{\sigma}_h^+ \cdot \boldsymbol{n}^+ + \boldsymbol{\sigma}_h^- \cdot \boldsymbol{n}^-.$$

On the interior edges, we therefore have

$$\begin{aligned} 0 = \langle \widehat{\boldsymbol{\sigma}_h} \cdot \boldsymbol{n}, \mu_h\rangle_{\partial\mathcal{T}_h \setminus \Gamma} &:= \sum_{K\in\mathcal{T}_h} \sum_{e\in\mathcal{E}(K)\cap\mathcal{E}_h^i} \langle \widehat{\boldsymbol{\sigma}_h} \cdot \boldsymbol{n}, \mu_h\rangle_e\,, \\ &= \sum_{\substack{e\in\mathcal{E}_h^i \\ e=\partial K_+\cap\partial K_-}} \left\langle \widehat{\boldsymbol{\sigma}_h}^+ \cdot \boldsymbol{n}^+ + \widehat{\boldsymbol{\sigma}_h}^- \cdot \boldsymbol{n}^-, \mu_h \right\rangle_e\,, \\ &= \sum_{e\in\mathcal{E}_h^i} \langle [\![\widehat{\boldsymbol{\sigma}_h}]\!], \mu_h\rangle_e = 0. \end{aligned} \tag{11}$$

All of the terms involved in the definition of $\widehat{\boldsymbol{\sigma}_h}$, given in (9), are polynomial quantities of degree up to k. Hence, we can conclude that both $\widehat{\boldsymbol{\sigma}_h}$ and $[\![\widehat{\boldsymbol{\sigma}_h}]\!]$ are

also polynomials of degree up to k. On the interior edges, (11) states that $[\![\widehat{\boldsymbol{\sigma}_h}]\!]$ is orthogonal to all of the polynomials of degree up to k, which leads to $[\![\widehat{\boldsymbol{\sigma}_h}]\!] \equiv 0$.

Remark 3.1: The transmission condition (10) can be understood as weak requirement of $\boldsymbol{H}_{\mathrm{div}}(\mathcal{O})$-conformity for $\boldsymbol{\sigma}_h$ and of $H^1(\mathcal{O})$-conformity for p_h. The continuity requirement for p_h is easily understood as the penalization term $\tau(p_h - \widehat{p_h})$ ensures that p_h and $\widehat{p_h}$ stay close to each another, as they are two approximations of the same physical quantity on ∂K, *i.e.* $p_h|_{\partial K} \simeq \widehat{p_h}|_{\partial K}$. For $\boldsymbol{\sigma}_h$, we use the following characterization of $\boldsymbol{H}_{\mathrm{div}}(\mathcal{O})$-conformity: it is shown in [PE12, Lemma 1.2.4] that $\boldsymbol{\sigma}_h \in \boldsymbol{H}_{\mathrm{div}}(\mathcal{O})$ means

$$\forall K \in \mathcal{T}_h,\ \boldsymbol{\sigma}_h^K \in \boldsymbol{H}_{\mathrm{div}}(K) \quad \text{and} \quad \forall e \in \mathcal{E}_h^i,\ [\![\boldsymbol{\sigma}_h]\!]_e \equiv 0.$$

The former is a consequence of the polynomial nature of the approximation spaces, and we will now focus on the latter. Owing to the transmission condition, we have

$$\forall e \in \mathcal{E}_h^i,\ 0 = [\![\widehat{\boldsymbol{\sigma}_h}]\!] = [\![\boldsymbol{\sigma}_h]\!] + i\omega[\![\tau(p_h - \widehat{p_h})]\!].$$

As p_h and $\widehat{p_h}$ are two approximations of the same unknown p, the quantity $p_h - \widehat{p_h}$ is expected to be small. We can therefore conclude that $[\![\boldsymbol{\sigma}_h]\!]$ is small and that

$$[\![\boldsymbol{\sigma}_h]\!] \underset{h_K \to 0}{\longrightarrow} 0.$$

For applications where a precise approximation of the flux is required, it is possible to post-process $\boldsymbol{\sigma}_h$ to obtain a new approximate $\widetilde{\boldsymbol{\sigma}_h}$ with strong $\boldsymbol{H}_{\mathrm{div}}$-conformity, see [CGS10, Sec. 5.1].

Remark 3.2: The equation (8b) can be rewritten as

$$-\omega^2 \left(\rho_0 p_h, w_h\right)_K + \left(\mathrm{div}\left(\boldsymbol{\sigma}_h\right), w_h\right)_K + i\omega \left\langle \tau(p_h - \widehat{p_h}), w_h \right\rangle_{\partial K} = \left(s, w_h\right)_K .$$

The boundary term weakly enforces the Dirichlet boundary condition

$$p_h = \widehat{p_h}, \quad \text{on } \partial K,$$

and the local problem (8a)–(8b) should therefore be interpreted as a Dirichlet solver on K. We will prove in Theorem 5.1 that this defines a discrete *local solver* when ωh_K is small enough.

3.3. **Condensed formulation.** HDG methods are usually stated in a compact form that can be obtained by summing the local problems (8a)–(8b) over the mesh elements and by adding the transmission condition (10). This formulation then reads : seek $(\boldsymbol{\sigma}_h, p_h, \widehat{p_h}) \in \boldsymbol{V}_h \times W_h \times M_h$ such that

$$(\boldsymbol{W_0}\boldsymbol{\sigma}_h, \boldsymbol{r}_h)_{\mathcal{T}_h} - (p_h, \mathrm{div}\left(\boldsymbol{r}_h\right))_{\mathcal{T}_h} + 2i\omega \left(p_h \boldsymbol{W_0} \boldsymbol{b_0}, \boldsymbol{r}_h\right)_{\mathcal{T}_h} = -\left\langle \widehat{p_h}, \boldsymbol{r}_h \cdot \boldsymbol{n} \right\rangle_{\partial \mathcal{T}_h}, \tag{12a}$$

$$-\omega^2 \left(\rho_0 p_h, w_h\right)_{\mathcal{T}_h} - \left(\boldsymbol{\sigma}_h, \nabla w_h\right)_{\mathcal{T}_h} + \left\langle \widehat{\boldsymbol{\sigma}_h} \cdot \boldsymbol{n}, w_h \right\rangle_{\partial \mathcal{T}_h} = \left(s, w_h\right)_{\mathcal{T}_h}, \tag{12b}$$

$$\left\langle \boldsymbol{\sigma}_h \cdot \boldsymbol{n} + i\omega\tau(p_h - \widehat{p_h}), \mu_h \right\rangle_{\partial \mathcal{T}_h} - \left\langle g_N, \mu_h \right\rangle_{\Gamma} = 0, \tag{12c}$$

for all $(\boldsymbol{r}_h, w_h, \mu_h) \in \boldsymbol{V}_h \times W_h \times M_h$.

Remark 3.3: At this point, to completely define the HDG method, it only remains to choose the penalization parameter τ, this will be done in Proposition 4.3 of Section 4.

The compact formulation (12a)–(12b)–(12c) is useful to perform the analyis of the method, however it cannot directly be used to obtain an efficient implementation. Indeed, with this formulation it is not clear how the local unknowns can be eliminated to obtain a problem for $\widehat{p_h}$ only. To emphasize how this can be done, we will now write a *condensed* variational formulation for $\widehat{p_h}$ only which is equivalent to the formulation (12a)–(12b)–(12c).
We introduce the so-called *local solvers*

$$\begin{aligned}
&\mathsf{P}^K : (\widehat{p_h}, s) \longmapsto p_h^K, \\
&\mathbf{\Sigma}^K : (\widehat{p_h}, s) \longmapsto \boldsymbol{\sigma}_h^K, \\
&\widehat{\mathbf{\Sigma}}^K : (\widehat{p_h}, s) \longmapsto \widehat{\boldsymbol{\sigma}_h}^K := \mathbf{\Sigma}^K(\widehat{p_h}, s) \cdot \boldsymbol{n}^K + i\omega\tau(\mathsf{P}^K(\widehat{p_h}, s) - \widehat{p_h}),
\end{aligned}$$

where $(\boldsymbol{\sigma}_h^K, p_h^K)$ is the solution of (8a)–(8b) and $\widehat{\boldsymbol{\sigma}_h}^K$ is defined by (9). Those local solvers are actually well-defined, this will be proven in Theorem 5.1. We can therefore rewrite the transmission condition (12c) as a variational problem on the skeleton of the mesh:

$$\text{(13)} \qquad \text{Seek } \widehat{p_h} \in M_h \text{ such that } \; a_h(\widehat{p_h}, \mu_h) = \ell_h(\mu_h), \; \text{for all } \mu_h \in M_h,$$

where

$$\begin{aligned}
a_h(\widehat{p_h}, \mu_h) &:= \left\langle \mathbf{\Sigma}^K(\widehat{p_h}, s) \cdot \boldsymbol{n} + i\omega\tau(\mathsf{P}^K(\widehat{p_h}, s) - \widehat{p_h}), \mu_h \right\rangle_{\partial\mathcal{T}_h}, \\
\ell_h(\mu_h) &:= \langle g_N, \mu_h \rangle_\Gamma .
\end{aligned}$$

Equation (13) is the so-called *global problem* and is the main equation of the HDG method.
As the local solvers satisfy the local problems (8a)–(8b), it is possible to show that the bilinear form of the global problem satisfies

$$\begin{aligned}
a_h(\widehat{p_h}, \mu_h) = &\left(\boldsymbol{W_0}\mathbf{\Sigma}^K(\widehat{p_h}), \mathbf{\Sigma}^K(\mu_h)\right)_{\mathcal{T}_h} - \omega^2 \left(\rho_0 \mathsf{P}^K(\widehat{p_h}), \mathsf{P}^K(\mu_h)\right)_{\mathcal{T}_h} \\
&+ 2i\omega \left(\boldsymbol{W_0 b_0} \cdot \mathbf{\Sigma}^K(\widehat{p_h}), \mathbf{\Sigma}^K(\mu_h)\right)_{\mathcal{T}_h} \\
&+ i\omega \left\langle \tau(\mathsf{P}^K(\widehat{p_h}) - \widehat{p_h}), \mathsf{P}^K(\mu_h) - \mu_h \right\rangle_{\partial\mathcal{T}_h},
\end{aligned}$$

by following [CGL09, Sec. 2.3]. With this characterization, we can see that the global problem has the structure of a convected Helmholtz equation. In particular testing with $\mu_h = \widehat{p_h}$ leads to a discrete global Garding-like inequality.
From a computational point of view, we proceed as described in Algorithm 1.

Algorithm 1: Solving HDG-$\boldsymbol{\sigma}_h$

for $K \in \mathcal{T}_h$ **do**
  `/* Assembling step */`
  Construct the local solvers P^K, $\mathbf{\Sigma}^K$, $\widehat{\mathbf{\Sigma}}^K$
  Add local contribution to the global problem (13)
Solve (13) for $\widehat{p_h}$ `// Main linear system to solve`
for $K \in \mathcal{T}_h$ **do**
  `/* Reconstruction step */`
  Reconstruct the local unknowns $p_h^K = \mathsf{P}^k(\widehat{p_h}, s)$ and $\boldsymbol{\sigma}_h^K = \mathbf{\Sigma}(\widehat{p_h}, s)$

This algorithm is the blueprint of the practical implementation of the HDG method which is discussed in [Rou21].

4. Choice of penalization parameter

The construction of the HDG method (12a)–(12b)–(12c) is not quite complete as the stabilization parameter τ has not been fixed yet. In this section, we present a way to chose τ that exploits the hyperbolic nature of the transient counterpart to (7a)–(7b). To this end, the HDG method (12a)–(12b)–(12c) is rewritten as a mixed DG method whose numerical fluxes are computed by solving a Riemann problem on the interface between two elements. Following the terminology of the Finite Volume and Discontinuous Galerkin communities, see *e.g.* [LeV02, Sec. 4.8] and [HW08, Sec. 2.4], we call those numerical fluxes (and the associated values for τ) *upwind*.

4.1. Mixed DG formulations.

In this section, we consider a mixed DG formulation for the convected Helmholtz equation. We begin with the discrete weak formulation of (7a)–(7b) on an element $K \in \mathcal{T}_h$

$$\int_K \boldsymbol{W_0}\boldsymbol{\sigma}_h^K \cdot \overline{\boldsymbol{r}_h} \mathrm{d}\boldsymbol{x} - \int_K p_h \mathrm{div}\,(\overline{\boldsymbol{r}_h})\,\mathrm{d}\boldsymbol{x} + 2i\omega \int_K p_h \boldsymbol{W_0}\boldsymbol{b_0} \cdot \overline{\boldsymbol{r}_h} \mathrm{d}\boldsymbol{x} = -\int_{\partial K} \widehat{p_h}\overline{\boldsymbol{r}_h} \cdot \boldsymbol{n} \mathrm{d}\sigma,$$
$$-\omega^2 \int_K \rho_0 p_h \overline{w_h} \mathrm{d}\boldsymbol{x} - \int_K \boldsymbol{\sigma}_h \cdot \nabla \overline{w_h} \mathrm{d}\boldsymbol{x} + \int_{\partial K} \overline{w_h}\widehat{\boldsymbol{\sigma}_h} \cdot \boldsymbol{n} \mathrm{d}\sigma = \int_K s\overline{w_h} \mathrm{d}\boldsymbol{x},$$

where $p_h \in W_h(K) := \mathcal{P}_k(K)$, $\boldsymbol{\sigma}_h \in \boldsymbol{V}_h(K) := \boldsymbol{\mathcal{P}}_k(K)$ and $\widehat{p_h}$ and $\widehat{\boldsymbol{\sigma}_h}$ are the *numerical fluxes* that connect the elements together. Summing over the elements $K \in \mathcal{T}_h$ yields

$$(14a)\quad (\boldsymbol{W_0}\boldsymbol{\sigma}_h, \boldsymbol{r}_h)_{\mathcal{T}_h} - (p_h, \mathrm{div}\,(\boldsymbol{r}_h))_{\mathcal{T}_h} + 2i\omega\,(p_h \boldsymbol{W_0}\boldsymbol{b_0}, \boldsymbol{r}_h)_{\mathcal{T}_h} + \langle \widehat{p_h}, \boldsymbol{r}_h \cdot \boldsymbol{n}\rangle_{\partial\mathcal{T}_h} = 0$$
$$(14b)\quad -\omega^2\,(\rho_0 p_h, w_h)_{\mathcal{T}_h} - (\boldsymbol{\sigma}_h, \nabla w_h)_{\mathcal{T}_h} + \langle \widehat{\boldsymbol{\sigma}_h} \cdot \boldsymbol{n}, w\rangle_{\partial\mathcal{T}_h} = (s, \boldsymbol{r}_h)_{\mathcal{T}_h}\,.$$

All the mixed DG methods can be generated from (14a)–(14b) by choosing he numerical fluxes $\widehat{p_h}$ and $\widehat{\boldsymbol{\sigma}_h}$. The choice of these numerical fluxes is important as they have an important impact on the quality of the numerical results.
To illustrate this, let us consider usual DG numerical fluxes, which can be expressed as

$$(15)\quad \widehat{p_h} = \{\!\{p_h\}\!\} + \boldsymbol{\alpha} \cdot [\![p_h]\!] + \beta [\![\boldsymbol{\sigma}_h]\!] \quad \text{and} \quad \widehat{\boldsymbol{\sigma}_h} = \{\!\{\boldsymbol{\sigma}_h\}\!\} + \boldsymbol{\gamma}[\![\boldsymbol{\sigma}_h]\!] + \delta[\![p_h]\!],$$

where $\boldsymbol{\alpha}, \boldsymbol{\gamma}$ are complex vectors and β, δ are complex numbers which determine the nature of the resulting DG method. For example, taking $\alpha = \beta = \gamma = 0$ leads to the DG method with *central fluxes* and taking $\beta = 0$ leads to the *Local Discontinuous Galerin* (LDG) method introduced in [CS98]. Both of those examples are detailed in [HW08, Sec. 7.2.2].
For DG methods, the numerical fluxes are usually defined on the interface between two elements. On the other hand, for HDG methods the numerical flux $\widehat{\boldsymbol{\sigma}}$ can be expressed only as a function of the local solution $(\boldsymbol{\sigma}_h^K, p_h^K)$ and of the numerical trace $\widehat{p_h}$:

$$(16)\quad \widehat{\boldsymbol{\sigma}_h}^{K,e} \cdot \boldsymbol{n}^{K,e} = \boldsymbol{\sigma}_h^K \cdot \boldsymbol{n} + i\omega\tau(p_h^K - \widehat{p_h}),$$

With this *elementary flux* defined on edge e of element K, it is possible to introduce a *local problem*. The normal continuity of the numerical fluxes is then ensured by adding an explicit continuity requirement in the numerical method

$$[\![\widehat{\boldsymbol{\sigma}_h}]\!] = 0 \iff \widehat{\boldsymbol{\sigma}_h}^{K_+,e} \cdot \boldsymbol{n}^{K_+,e} = -\widehat{\boldsymbol{\sigma}_h}^{K_-,e} \cdot \boldsymbol{n}^{K_-,e},$$

where $e = \partial K_+ \cap \partial K_-$. In. SECTION 3, no value was chosen for the parameter τ of (16). We will now present a way to choose this value with physical meaning. The following proposition links the expressions of the elementary HDG fluxes (16) and of the DG fluxes $\widehat{p_h}$ and $\widehat{\boldsymbol{\sigma}_h}$ of (15).

Proposition 4.1. *The HDG method* (12a)–(12b)–(12c) *of* SECTION 3 *with the* elementary fluxes *of* (16) *is equivalent to a mixed DG method* (14a)–(14b) *with fluxes* (15)*, where*

$$\widehat{p_h} = \{\!\{p_h\}\!\} + \frac{\tau^+\boldsymbol{n}^+ + \tau^-\boldsymbol{n}^-}{2(\tau^+ + \tau^-)} \cdot [\![p_h]\!] + \frac{1}{i\omega(\tau^+ + \tau^-)}[\![\boldsymbol{\sigma}_h]\!], \tag{17a}$$

$$\widehat{\boldsymbol{\sigma}_h} = \{\!\{\boldsymbol{\sigma}_h\}\!\} + i\omega\frac{\tau^+\tau^-}{\tau^+ + \tau^-}[\![p_h]\!] - \frac{\tau^+\boldsymbol{n}^+ + \tau^-\boldsymbol{n}^-}{2(\tau^+ + \tau^-)}[\![\boldsymbol{\sigma}_h]\!], \tag{17b}$$

or equivalently

$$\boldsymbol{\alpha} = \frac{\tau^+\boldsymbol{n}^+ + \tau^-\boldsymbol{n}^-}{2(\tau^+\tau^-)},\ \beta = \frac{1}{i\omega(\tau^+ + \tau^-)},\ \boldsymbol{\gamma} = i\omega\frac{\tau^+\tau^-}{\tau^+ + \tau^-},\ \delta = -\frac{\tau^+\boldsymbol{n}^+ + \tau^-\boldsymbol{n}^-}{2(\tau^+ + \tau^-)},$$

for all interior edges $\mathcal{E}_h^i \ni e = \partial K_+ \cap \partial K_-$ *and where* $\tau^\pm = \tau|_{\partial K_\pm}$.

Proof: The proof of PROPOSITION 4.1 is a straightforward adaptation of the proof of [PE12, Lemma 4.42] as the only differences are the $i\omega$ factors.

We would like to point out that the particular form of $\widehat{p_h}$ makes the HDG method actually hybridizable. Indeed for the LDG and central fluxes methods, as described in [HW08, Sec. 7.2.2], testing with $[\boldsymbol{r}_h, 0]$ shows that the quantity $\boldsymbol{\sigma}_h$ is completely defined in terms of p_h as $\boldsymbol{\sigma}_h = -\boldsymbol{K_0}\nabla p_h + \mathcal{L}(p_h)$ where $\mathcal{L}$ is a *lifting operator*. It is therefore possible to eliminate $\boldsymbol{\sigma}_h$ locally, which makes the hybridization process impossible. On the other hand, in the HDG method, the elementary flux depends on $\widehat{p_h}$ and we obtain a *transmission condition* that enforces the normal continuity of $\widehat{\boldsymbol{\sigma}_h}$ on the interface between two elements. This condition is global as it contains the coupling between unknowns on different elements and allows the local elimination of the original unknowns $(\boldsymbol{\sigma}_h, p_h)$ to obtain a global problem for $\widehat{p_h}$ only.

4.2. **Computing of the upwind DG fluxes.** The choice of the numerical fluxes has a major influence on the properties of the resulting DG method. In this subsection, we compute physically informed numerical fluxes that are used to construct an *upwind* DG method for the convected Helmholtz equation. To compute those upwind fluxes, we need to define the value of the solution on the interface between two elements, and we therefore need to solve the associated Riemann problem. After computing those fluxes, we show that the resulting upwind DG method is actually hybridizable and that we can therefore construct an upwind HDG method for the convected Helmholtz equation.

Proposition 4.2. *The* upwind DG fluxes *are given by*

$$\widehat{p_h} = \{\!\{p\}\!\} - \frac{\boldsymbol{v_0}}{2c_0} \cdot [\![p]\!] + \frac{1}{2i\omega\rho_0 c_0}[\![\boldsymbol{\sigma}]\!] \tag{18a}$$

$$\widehat{\boldsymbol{\sigma}} = \{\!\{\boldsymbol{\sigma}\}\!\} + \frac{\boldsymbol{v_0}}{2c_0}[\![\boldsymbol{\sigma}]\!] + i\omega\rho_0\frac{c_0^2 - (\boldsymbol{v_0}\cdot\boldsymbol{n}^-)^2}{2c_0}[\![p]\!]. \tag{18b}$$

To prove this proposition, we solve a Riemann problem and compare its solution with PROPOSITION 4.1 to obtain a value for $\tau^\pm$ with physical meaning. The first step to be able to solve the Riemann problem is to rewrite the original equation as

a time-domain hyperbolic system. The remaining of this section is devoted to the proof of Proposition 4.2.

4.2.1. *Hyperbolic system.* We start from time-domain counterpart to (4)

$$\rho_0 \frac{\partial^2 p}{\partial t^2} - \operatorname{div}\left(\boldsymbol{K_0} \nabla p - 2\rho_0 \frac{\partial p}{\partial t} \boldsymbol{v_0} \right) = 0.$$

For simplicity's sake, we continue to note the unknowns in the same way, whereas in all rigor we should adopt a notation specific to the time domain. We therefore introduce the *total flux*

$$\frac{\partial \widetilde{\boldsymbol{\sigma}}}{\partial t} = -\boldsymbol{K_0} \nabla p + 2\rho_0 \frac{\partial p}{\partial t} \boldsymbol{v_0},$$

leading to the following first-order formulation

$$\frac{\partial p}{\partial t} = -\frac{1}{\rho_0} \operatorname{div}\left(\widetilde{\boldsymbol{\sigma}} \right), \tag{19a}$$

$$\frac{\partial \widetilde{\boldsymbol{\sigma}}}{\partial t} = -\boldsymbol{K_0} \nabla p - 2 \operatorname{div}\left(\widetilde{\boldsymbol{\sigma}} \right) \boldsymbol{v_0}. \tag{19b}$$

We have introduced the unknown $\widetilde{\boldsymbol{\sigma}}$ to obtain a first-order hyperbolic system, and have the following relationship between $\boldsymbol{\sigma}$ and $\widetilde{\boldsymbol{\sigma}}$

$$\boldsymbol{\sigma} = i\omega \widetilde{\boldsymbol{\sigma}},$$

making it possible to go back to a second-order in frequency formulation.
The system (19a)–(19b) can be written as

$$\frac{\partial}{\partial t} \begin{bmatrix} p \\ \widetilde{\boldsymbol{\sigma}} \end{bmatrix} = \mathbb{A}_x \frac{\partial}{\partial x} \begin{bmatrix} p \\ \widetilde{\boldsymbol{\sigma}} \end{bmatrix} + \mathbb{A}_y \frac{\partial}{\partial y} \begin{bmatrix} p \\ \widetilde{\boldsymbol{\sigma}} \end{bmatrix}, \tag{20}$$

where

$$\mathbb{A}_x := \begin{bmatrix} 0 & -\frac{1}{\rho_0} & 0 \\ -M_{0,xx} & -2v_{0,x} & 0 \\ -M_{0,yx} & -2v_{0,y} & 0 \end{bmatrix} \quad \text{and} \quad \mathbb{A}_y := \begin{bmatrix} 0 & 0 & -\frac{1}{\rho_0} \\ -M_{0,xy} & 0 & -2v_{0,x} \\ -M_{0,yy} & 0 & -2v_{0,y} \end{bmatrix}.$$

4.2.2. *Riemann solver.* We consider a vertical interface located at $x = 0$ and we assume that the background flow is uniform. As $\boldsymbol{\sigma} \in \boldsymbol{H}_{\operatorname{div}}(\mathcal{O})$, the communication between the two subdomains only occurs in the direction which is normal to the interface, *i.e.* in the x-direction. The system (20) therefore reduces to the following 1D problem

$$\frac{\partial \mathbf{U}}{\partial t} = \mathbb{A} \frac{\partial \mathbf{U}}{\partial x}, \tag{21a}$$

where

$$\mathbf{U} := \begin{bmatrix} p \\ \widetilde{\sigma_x} \end{bmatrix}, \quad \text{and} \quad \mathbb{A} := \begin{bmatrix} 0 & -\frac{1}{\rho_0} \\ -M_{0,xx} & -2v_{0,x} \end{bmatrix}.$$

The solution of this 1D problem will be used to infer the expression for the numerical flux on any interface between two elements.
We will solve the problem (21a) with the following initial condition

$$\mathbf{U}(x,0) = \mathbf{U}^+, \qquad \text{if } x > 0, \tag{21b}$$

$$\mathbf{U}(x,0) = \mathbf{U}^-, \qquad \text{if } x < 0. \tag{21c}$$

With this choice of initial condition, we obtain a well-posed problem which is invariant with respect to y. Our goal is to compute $\mathbf{U}$ at $x = 0$. As the system is hyperbolic, $\mathbb{A}$ can be diagonalized and the system reduces to two advection equations that can be solved using the method of characteristics. The solution at $x = 0$ can then be expressed as the superposition of the right-going mode coming from the left and of the left-going mode coming from the right. To compute the eigenvalues of $\mathbb{A}$, we solve

$$\begin{vmatrix} -\lambda & -\frac{1}{\rho_0} \\ -M_{0,xx} & -2v_{0,x} - \lambda \end{vmatrix} = 0 \iff \lambda^2 + 2v_{0,x}\lambda - \frac{M_{0,xx}}{\rho_0} = 0.$$

Recalling that

$$M_{0,xx} = \rho_0 c_0^2 - \rho_0 v_{0,x}^2,$$

we obtain the two following eigenvalues

$$\lambda_1 = -\left(c_0 + v_{0,x}\right),$$
$$\lambda_2 = c_0 - v_{0,x},$$

and the associated eigenvectors are

$$\boldsymbol{w}_1 := \begin{bmatrix} 1 \\ \rho_0(c_0 + v_{0,x}) \end{bmatrix} \quad \text{and} \quad \boldsymbol{w}_2 := \begin{bmatrix} 1 \\ \rho_0(v_{0,x} - c_0). \end{bmatrix}$$

The solution to (21a)–(21b)–(21c) is expressed as follows

$$\mathbf{U}(x,t) = \mathbf{U}_1(x,t)\boldsymbol{w}_1 + \mathbf{U}_2(x,t)\boldsymbol{w}_2$$

The eigenvector coefficients are $\mathbf{U}_i(x,t) = \mathbf{U}_i(x - \lambda_i t, 0)$ since they each solve a scalar transport equation

$$\frac{\partial \mathbf{U}}{\partial t}(x,t) + \mathbb{A}\frac{\partial \mathbf{U}}{\partial x}(x,t) = \mathbf{0} \iff \frac{\partial \mathbf{U}_i}{\partial t}(x,t) + \lambda_i \frac{\partial \mathbf{U}_i}{\partial x}(x,t) = 0, \forall i,$$

As $\lambda_1 < 0$, $\boldsymbol{w}_1$ is a left-propagating mode, and as $\lambda_2 > 0$, $\boldsymbol{w}_2$ is a right-propagating mode.
We denote by $\hat{\mathbf{U}} := [\hat{p}, \hat{\widetilde{\sigma}}_x]^T$ the value of $\mathbf{U}$ at $x = 0$ and $t > 0$. It can be expressed as the superposition of the right-propagating mode associated to λ_2 coming from the left and of the left-propagating mode associated to λ_1 coming from the right, so we have

$$\hat{\mathbf{U}}(t) = \mathbf{U}_1(-\lambda_1 t, 0)\boldsymbol{w}_1 + \mathbf{U}_2(-\lambda_2 t, 0)\boldsymbol{w}_2$$

Taking into account the initial condition of the Riemann problem, we get

$$\mathbf{U}_1(x,0) = \left(\frac{1}{2} - \frac{v_{0,x}}{2c_0}\right) p(x,0) + \frac{1}{2\rho_0 c_0}\widetilde{\sigma}_x(x,0), \text{ for } x > 0,$$
$$\mathbf{U}_2(x,0) = \left(\frac{1}{2} + \frac{v_{0,x}}{2c_0}\right) p(x,0) - \frac{1}{2\rho_0 c_0}\widetilde{\sigma}_x(x,0), \text{ for } x < 0,$$

and $\widehat{\mathbf{U}}$ can the be expressed as

$$\widehat{p} = \frac{1}{2}\left(p^+ + p^-\right) - \frac{v_{0,x}}{2c_0}\left(p^+ - p^-\right) + \frac{1}{2\rho_0 c_0}\left(\widetilde{\sigma}_x^+ - \widetilde{\sigma}_x^-\right),$$
$$\widehat{\widetilde{\sigma}_x} = \frac{1}{2}\left(\widetilde{\sigma}_x^+ + \widetilde{\sigma}_x^-\right) + \frac{v_{0,x}}{2c_0}\left(\widetilde{\sigma}_x^+ - \widetilde{\sigma}_x^-\right) + \rho_0\frac{c_0^2 - v_{0,x}^2}{2c_0}\left(p^+ - p^-\right),$$

where $p^\pm(t) = p(0^\pm, t)$.
Finally, we can infer the form of the DG flux for a generic interface

$$\widehat{p} = \{\!\{p\}\!\} - \frac{1}{2c_0}\boldsymbol{v_0}\cdot[\![p]\!] + \frac{1}{2\rho_0 c_0}[\![\widetilde{\boldsymbol{\sigma}}]\!], \tag{23a}$$

$$\widehat{\widetilde{\boldsymbol{\sigma}}} = \{\!\{\widetilde{\boldsymbol{\sigma}}\}\!\} + \frac{\boldsymbol{v_0}}{2c_0}[\![\widetilde{\boldsymbol{\sigma}}]\!] + \rho_0\frac{c_0^2 - (\boldsymbol{v_0}\cdot\boldsymbol{n}^-)^2}{2c_0}[\![p]\!]. \tag{23b}$$

Rewriting (23a)–(23b) in terms of $\boldsymbol{\sigma}$ instead of $\widetilde{\boldsymbol{\sigma}}$ leads to

$$\widehat{p_h} = \{\!\{p\}\!\} - \frac{1}{2c_0}\boldsymbol{v_0}\cdot[\![p]\!] + \frac{1}{2i\omega\rho_0 c_0}[\![\boldsymbol{\sigma}]\!]$$
$$\widehat{\boldsymbol{\sigma}} = \{\!\{\boldsymbol{\sigma}\}\!\} + \frac{\boldsymbol{v_0}}{2c_0}[\![\boldsymbol{\sigma}]\!] + i\omega\rho_0\frac{c_0^2 - (\boldsymbol{v_0}\cdot\boldsymbol{n}^-)^2}{2c_0}[\![p]\!].$$

The above result provides us with a proof of Proposition 4.2.
Remark 4.1: The numerical fluxes presented in Proposition 4.2 are called *upwind* as they are associated with the solution of a Riemann problem between two elements. In the subsequent proof, we limit ourselves to the case of an interface in a homogeneous medium. Different upwind fluxes could be obtained by using a similar construction in a discontinuous medium.

4.3. **HDG flux and penalization parameter.** We can now obtain a relationship between the upwind fluxes and the HDG penalization parameter τ. We recall that, according to Proposition 4.1, the HDG fluxes are defined by

$$\widehat{p_h} = \{\!\{p_h\}\!\} + \frac{\tau^+\boldsymbol{n}^+ + \tau^-\boldsymbol{n}^-}{2(\tau^+ + \tau^-)}\cdot[\![p_h]\!] + \frac{1}{i\omega(\tau^+ + \tau^-)}[\![\boldsymbol{\sigma}_h]\!],$$
$$\widehat{\boldsymbol{\sigma}_h} = \{\!\{\boldsymbol{\sigma}_h\}\!\} + i\omega\frac{\tau^+\tau^-}{\tau^+ + \tau^-}[\![p_h]\!] - \frac{\tau^+\boldsymbol{n}^+ + \tau^-\boldsymbol{n}^-}{2(\tau^+ + \tau^-)}[\![\boldsymbol{\sigma}_h]\!].$$

Proposition 4.3. *On an interior face $\mathcal{E}_h^i \ni e = \partial K_+ \cap \partial K_-$ the penalization parameter associated with the upwind DG fluxes is given by*

$$\tau^\pm = \rho_0(c_0 + \boldsymbol{v_0}\cdot\boldsymbol{n}^\pm), \tag{25}$$

where $\tau^\pm = \tau|_{\partial K_\pm}$.

Proof: Comparing (18a)–(18b) with (17a)–(17b) , we see that

$$\tau^+ + \tau^- = 2\rho_0 c_0 \quad \text{and} \quad \frac{\tau^+\tau^-}{\tau^+ + \tau^-} = \rho_0\frac{c_0^2 - (\boldsymbol{v_0}\cdot\boldsymbol{n}^-)^2}{2c_0}.$$

The last system leads to the following second-order equation

$$(\tau^+)^2 - 2\rho_0 c_0\tau^+ + \rho_0^2\left(c_0^2 - (\boldsymbol{v_0}\cdot\boldsymbol{n}^-)^2\right) = 0,$$

and to the two following families for $\tau^\pm$

$$\tau_1^+ = \rho_0(c_0 + \boldsymbol{v_0}\cdot\boldsymbol{n}^-), \qquad \tau_1^- = \rho_0(c_0 - \boldsymbol{v_0}\cdot\boldsymbol{n}^-),$$
$$\tau_2^+ = \rho_0(c_0 - \boldsymbol{v_0}\cdot\boldsymbol{n}^-), \qquad \tau_2^- = \rho_0(c_0 + \boldsymbol{v_0}\cdot\boldsymbol{n}^-).$$

To discriminate between $\tau_1^{\pm}$ and $\tau_2^{\pm}$ we once again go back to (17a)–(17b) and we see that the solution must satisfy

$$-\frac{\boldsymbol{v_0}\cdot\boldsymbol{n}^-}{2c_0} = \left(\frac{\tau^+\boldsymbol{n}^+ + \tau^-\boldsymbol{n}^-}{2(\tau^+ + \tau^-)}\right)\cdot\boldsymbol{n}^- = -\frac{\tau^+ - \tau^-}{2(\tau^+ + \tau^-)}.$$

We can therefore conclude that the upwind fluxes are obtained by using the $\tau_2^{\pm}$ solution. We can make this choice independent of the orientation convention by noticing that $\boldsymbol{n}^+ = -\boldsymbol{n}^-$, leading to

$$\tau_2^{\pm} = \rho_0(c_0 + \boldsymbol{v_0}\cdot\boldsymbol{n}^{\pm}).$$

This is a natural choice as the terms involving τ will be computed on each element. It is therefore convenient to have an expression in terms of the local outgoing normal vector to the boundary rather than an expression depending on the orientation of the edges, which is a global piece of information.

Remark 4.2: To keep polynomial fluxes on the interfaces, the background quantities will be approximated by their value at the center of the interface.

Remark 4.3: In the context of DG and HDG methods, τ is usually chosen to be of the «order of unity» to ensure optimal convergence rate. In the error analysis of the method, we allow the dependency to the background coefficient to be hidden in the constants, so the choice (25) is actually possible.

5. Local solvability

We will now show the local solvability for the proposed *total flux* formulation based HDG method (12a)–(12b)–(12c). Proving the well-posedness of the local problems is always very important when working with HDG methods. For strongly coercive problems, for which HDG methods were initially designed, this property usually comes directly from the continuous problem. However for harmonic wave equations, which are only weakly coercive, things are more complicated: indeed solving the local problem amounts to solving a wave problem with Dirichlet boundary conditions. We therefore need to ensure that the local problem does not introduce resonance into the method, which is the case when the elements are small enough. In this section, we will prove that the static condensation process is well-defined when the mesh is fine enough.

In this section, we will make frequent use of the notation $a \lesssim b$, which is an abbreviation for

$$a \lesssim b \iff \exists C > 0,\ C \text{ independent of } h, \text{ such that } \ a \leqslant Cb.$$

We would like to point out that we will not establish frequency-explicit error estimates, and that we therefore allow ω to be hidden inside $\lesssim$. For more details on frequency-explicit analysis of numerical method for harmonic wave propagation, we refer the reader to [CFN19]. We will also frequently use the following *absorption result* which holds when the mesh size h is small enough.

Lemma 5.1. *Let a, b, h be positive real numbers and c be a real number.*

(*i*) *If $a \lesssim ah + b$ and if h is small enough then $a \lesssim b$,*
(*ii*) *If $a^2 \lesssim ab + c$ then $a^2 \lesssim b^2 + c$.*

First, we need to prove two preliminary results.

Lemma 5.2. *For $p_h \in \mathcal{P}_k(K)$ with $k > 0$, the following inverse inequality holds*

$$\|\nabla p_h \cdot \boldsymbol{n}\|_{\partial K} \lesssim h_K^{-\frac{1}{2}} \|\nabla p_h\|_K .$$

Proof:
First, we notice that if p_h is constant, the desired inequality reduces to $0 \leqslant 0$. We therefore only consider non-constant p_h. For $\boldsymbol{u}_h \in \boldsymbol{\mathcal{P}}_k(K)$, we have

$$\|\boldsymbol{u}_h \cdot \boldsymbol{n}\|_{\partial K} \leqslant \|\boldsymbol{n}\|_\infty \|\boldsymbol{u}_h\|_{\partial K} \lesssim \|\boldsymbol{u}_h\|_{\partial K} ,$$

then using the discrete trace inequality [PE12, Lem. 1.46]

$$\|\boldsymbol{u}_h\|_{\partial K} \lesssim h^{-1/2} \|\boldsymbol{u}_h\|_K ,$$

and choosing $\boldsymbol{u}_h = \nabla p_h$, we obtain the desired estimate. ∎

Lemma 5.3. *If $p \in H^1(K)$ and $\boldsymbol{b_0} \in \boldsymbol{L}^\infty(K) \cap \boldsymbol{\mathcal{C}}(\mathcal{O})$, where $\boldsymbol{\mathcal{C}}(\mathcal{O})$ is the space of vector functions continuous in the domain $\mathcal{O}$, then the following identity holds*

$$\mathfrak{Re}\left(p\boldsymbol{b_0}, \nabla p\right)_K = \frac{1}{2} \langle (\boldsymbol{b_0} \cdot \boldsymbol{n}) p, p \rangle_{\partial K} .$$

Proof: As $\operatorname{div}(\boldsymbol{b_0}) = 0.$, we use an integration by parts to obtain a relationship between $\left(p\boldsymbol{b_0}, \nabla p\right)_K$ and its complex conjugate :

$$\begin{aligned} 2\mathfrak{Re}\left(p\boldsymbol{b_0}, \nabla p\right)_K &= \left(p\boldsymbol{b_0}, \nabla p\right)_K + \overline{\left(p\boldsymbol{b_0}, \nabla p\right)_K} \\ &= -\left(\operatorname{div}\left(p\boldsymbol{b_0}\right), p\right)_K + \langle (\boldsymbol{b_0} \cdot \boldsymbol{n}) p, p \rangle_{\partial K} + \left(\nabla p, p\boldsymbol{b_0}\right)_K \\ &= -\left(\boldsymbol{b_0} \cdot \nabla p, p\right)_K + \langle (\boldsymbol{b_0} \cdot \boldsymbol{n}) p, p \rangle_{\partial K} + \left(\boldsymbol{b_0} \cdot \nabla p, p\right)_K \\ &= \langle (\boldsymbol{b_0} \cdot \boldsymbol{n}) p, p \rangle_{\partial K} , \end{aligned}$$

∎

Theorem 5.1 (Local solvability)**.** *If $\tau \in \mathbb{R}$ is chosen such that*

$$\exists \tau_0 > 0, \quad \forall e \in \mathcal{E}(K), \quad 0 < \tau_0 \leqslant \tau - \boldsymbol{b_0} \cdot \boldsymbol{n},$$

then there exists a constant $\alpha_+ > 0$ such that the local problem is well-posed if $\omega h_K < \alpha_+$.

Proof: As (8a)–(8b) is a square finite-dimensional problem, we only need to prove uniqueness of the solution. We therefore assume that $\widehat{p_h} = 0$ and $s = 0$, and we need to show that the system

$$\text{(27a)} \quad \left(\boldsymbol{W_0}\boldsymbol{\sigma}_h, \boldsymbol{r}_h\right)_K - \left(p_h, \operatorname{div}\left(\boldsymbol{r}_h\right)\right)_K + 2i\omega \left(p_h \boldsymbol{W_0}\boldsymbol{b_0}, \boldsymbol{r}_h\right)_K = 0, \qquad \forall \boldsymbol{r}_h \in \boldsymbol{V}_h(K)$$

$$\text{(27b)} \quad -\omega^2 \left(\rho_0 p_h, w_h\right)_K + \left(\operatorname{div}\left(\boldsymbol{\sigma}_h\right), w_h\right)_K + i\omega \langle \tau p_h, w_h \rangle_{\partial K} = 0, \quad \forall w_h \in W_h(K),$$

has only one solution $(\boldsymbol{\sigma}_h, p_h) = (\boldsymbol{0}, 0)$.
Step 1: Energy-like identity.
We test (27a) with $\boldsymbol{r}_h = \boldsymbol{\sigma}_h$ and conjugate the resulting equation, we then test (27b) with $w_h = p_h$ and add the two resulting equations leading to

$$\text{(28)} \qquad \|\boldsymbol{\sigma}_h\|^2_{\boldsymbol{W_0},K} - \omega^2 \|p_h\|^2_{\rho_0,K} - 2i\omega \left(\boldsymbol{W_0}\boldsymbol{\sigma}_h, p_h \boldsymbol{b_0}\right)_K + i\omega \langle \tau p_h, p_h \rangle_{\partial K} = 0,$$

as $\boldsymbol{W_0}$ is real and symmetric. Taking $\boldsymbol{r}_h = p_h \{\boldsymbol{b_0}\}$, where $\{\boldsymbol{b_0}\}$ is the average of $\boldsymbol{b_0}$ on K, in (27a), we have

$$\left(\boldsymbol{W_0}\boldsymbol{\sigma}_h, p_h \{\boldsymbol{b_0}\}\right)_K - \left(p_h, \{\boldsymbol{b_0}\} \cdot \nabla p_h\right)_K + 2i\omega \left(p_h \boldsymbol{W_0}\boldsymbol{b_0}, p_h \{\boldsymbol{b_0}\}\right)_K = 0,$$

leading to

$$(\boldsymbol{W_0}\boldsymbol{\sigma}_h, p_h\boldsymbol{b_0})_K = (p_h, \boldsymbol{b_0}\cdot\nabla p_h)_K - 2i\omega\,(p_h\boldsymbol{W_0}\boldsymbol{b_0}, p_h\boldsymbol{b_0})_K + \varepsilon, \tag{29}$$

where

$$\varepsilon := (\boldsymbol{W_0}\boldsymbol{\sigma}_h, p_h\delta\boldsymbol{b_0})_K - (p_h, \delta\boldsymbol{b_0}\cdot\nabla p_h)_K + 2i\omega\,(p_h\boldsymbol{W_0}\boldsymbol{b_0}, p_h\delta\boldsymbol{b_0})_K\,,$$

with $\delta\boldsymbol{b_0} = \boldsymbol{b_0} - \{\boldsymbol{b_0}\}$. In *Step 2*, it will be proven that $|\varepsilon|$ is small. Then inserting (29) in (28), we obtain

$$\begin{aligned}\|\boldsymbol{\sigma}_h\|^2_{\boldsymbol{W_0},K} - \omega^2(\|p_h\|^2_{\rho_0,K} + 4\,\|p_h\boldsymbol{b_0}\|^2_{\boldsymbol{W_0},K}) \\ - 2i\omega\,(p_h, \boldsymbol{b_0}\cdot\nabla p_h)_K - 2i\omega\varepsilon + i\omega\,\langle\tau p_h, p_h\rangle_{\partial K} = 0\end{aligned} \tag{30}$$

Step 2: Estimating $|\varepsilon|$. To estimate $|\varepsilon|$ we use the regularity of $\boldsymbol{b_0}$. Indeed as $\boldsymbol{b_0}$ is Lipschitz continuous, we have $\boldsymbol{b_0}\in\boldsymbol{W}^{1,\infty}(\mathcal{O})$, then using the Poincaré-Wirtinger inequality we obtain

$$\|\delta\boldsymbol{b_0}\|_{\boldsymbol{L}^\infty(K)} = \|\boldsymbol{b_0} - \{\boldsymbol{b_0}\}\|_{\boldsymbol{L}^\infty(K)} \leqslant Ch_K\,\|\nabla\boldsymbol{b_0}\|_{\boldsymbol{L}^\infty(\mathcal{O})} \lesssim h_K,$$

where $\{u\}$ is the average value of u over K. This leads to

$$|\varepsilon| \lesssim h_K\,\|\boldsymbol{\sigma}_h\|_K\,\|p_h\|_K + h_K\,\|p_h\|_K\,\|\nabla p_h\|_K + h_K\,\|p_h\|^2_K\,.$$

Young's inequality yields

$$|\varepsilon| \lesssim h_K^2\,\|\boldsymbol{\sigma}_h\|^2_K + \|p_h\|^2_K + h_K^2\,\|\nabla p_h\|^2_K\,. \tag{31}$$

Taking the imaginary part of (30) leads to

$$-2\omega\mathfrak{Re}\,(p_h\boldsymbol{b_0}, \nabla p_h)_K + \omega\,\langle\tau p_h, p_h\rangle_{\partial K} = 2\omega\mathfrak{Re}\varepsilon.$$

Lemma 5.3 implies that

$$\langle(\tau - \boldsymbol{b_0}\cdot\boldsymbol{n})p_h, p_h\rangle_{\partial K} = 2\mathfrak{Re}\varepsilon.$$

As $0 < \tau_0 \leqslant \tau\ - \boldsymbol{b_0}\cdot\boldsymbol{n}$ where τ_0 does not depend on h_K, we have

$$\|p_h\|^2_{\partial K} \lesssim |\varepsilon| \lesssim\ h_K^2\,\|\boldsymbol{\sigma}_h\|^2_K + \|p_h\|^2_K + h_K^2\,\|\nabla p_h\|^2_K\,. \tag{32}$$

According to [EG04, Lemma B.63 & Example B.64] we have

$$\|p_h\|_K \leqslant C_K^2\,\|\nabla p_h\|^2_K + \Big(\frac{C_K}{\mathrm{meas}(\partial K)}\Big)^2\,\|p_h\|^2_{\partial K}\,,$$

with C_K the Poincaré constant[2] of K . Using standard scaling inequalities, we have

$$C_K \lesssim h_K \quad \text{and} \quad \frac{C_K}{\mathrm{meas}(\partial K)} \lesssim h_K^{\frac{1}{2}},$$

when the mesh is regular, see [EG04, Def. 1.107]. Using (32), this leads to

$$\|p_h\|^2_K \lesssim h_K^2\,\|\nabla p_h\|^2_K + h_K\,\|p_h\|^2_{\partial K} \lesssim h_K^2\,\|\nabla p_h\|^2_K + h_K^3\,\|\boldsymbol{\sigma}_h\|^2_K + h_K\,\|p_h\|^2_K\,.$$

Using the absorption argument of Lemma 5.1 for h_K small enough, we obtain

$$\|p_h\|^2_K \lesssim h_K^2\,\|\nabla p_h\|^2_K + h_K^3\,\|\boldsymbol{\sigma}_h\|^2_K\,. \tag{33}$$

It follows from (31) that

$$|\varepsilon| \lesssim h_K^2\,\Big(\|\boldsymbol{\sigma}_h\|^2_K + \|\nabla p_h\|^2_K\Big)\,. \tag{34}$$

Step 3: Estimating $\|\boldsymbol{\sigma}_h\|_K$

[2]The constant used by the authors of [EG04] is the inverse of the usual Poincaré constant.

Taking the real part of the Garding's identity (30), we have

$$\|\boldsymbol{\sigma}_h\|_K^2 \lesssim \|p_h\|_K^2 + \|p_h\|_K \|\nabla p_h\|_K + |\varepsilon| \lesssim \left(1 + \frac{1}{h_K}\right) \|p_h\|_K^2 + h_K \|\nabla p_h\|_K^2 + |\varepsilon|.$$

It follows from (33) and (34) that

$$\|\boldsymbol{\sigma}_h\|_K^2 \lesssim h_K \|\nabla p_h\|_K^2 + h_K^2 \|\boldsymbol{\sigma}_h\|_K^2 .$$

Lemma 5.1, leads to

$$\|\boldsymbol{\sigma}_h\|_K^2 \lesssim h_K \|\nabla p_h\|_K^2 . \tag{35}$$

Inserting the last inequality in (32) and (33), we therefore have

$$\|\boldsymbol{\sigma}_h\|_K \lesssim h_K^{\frac{1}{2}} \|\nabla p_h\|_K , \ \|p_h\|_K \lesssim h_K \|\nabla p_h\|_K \text{ and } \|p_h\|_{\partial K}^2 \lesssim h_K \|\nabla p_h\|_K . \tag{36}$$

Step 4: Conclusion. Taking $\boldsymbol{r}_h = \nabla p_h$ in (27a) and integrating by parts, we have

$$\begin{aligned} \|\nabla p_h\|_K^2 &= -\left(\boldsymbol{W_0}\boldsymbol{\sigma}_h, \nabla p_h\right)_K - 2i\omega \left(p_h \boldsymbol{W_0}\boldsymbol{b_0}, \nabla p_h\right)_K + \langle p_h, \nabla p_h \cdot \boldsymbol{n}\rangle_{\partial K} \\ &\lesssim \|\boldsymbol{\sigma}_h\|_K \|\nabla p_h\|_K + \|p_h\|_K \|\nabla p_h\|_K + \|p_h\|_{\partial K} \|\nabla p_h\|_{\partial K} \end{aligned}$$

Lemma 5.2 allows to write

$$\|\nabla p_h\|_K^2 \lesssim \|\boldsymbol{\sigma}_h\|_K \|\nabla p_h\|_K + \|p_h\|_K \|\nabla p_h\|_K + h_K^{-1/2} \|p_h\|_{\partial K} \|\nabla p_h\|_K$$

The inequalities (36) allows to write

$$\|\nabla p_h\|_K^2 \lesssim h_K^{\frac{1}{2}} \|\nabla p_h\|_K^2 .$$

Lemma 5.1 leads to $\nabla p_h = 0$. It follows from (36) that $p_h = 0$ and $\boldsymbol{\sigma}_h = 0$.

■

6. Error analysis

The error analysis of the HDG method for the standard Helmholtz equation has been carried out in [DS19, Sec. 3.5.1 & 3.5.2]. The convective terms introduces new difficulties that we address in this section. We give a complete proof in the case of Fourier boundary condition, *i.e.* $\Gamma_D = \varnothing$.

This error analysis relies on the tailored HDG projection that fits the structure of the numerical trace. The HDG projection $(\boldsymbol{\Pi}, \Pi)$

$$(\boldsymbol{\Pi}, \Pi) : \boldsymbol{H}_{\mathrm{div}}(\mathcal{O}) \times H^1(\mathcal{O}) \longrightarrow \boldsymbol{V}_h \times W_h := \boldsymbol{\mathcal{P}}_k(\mathcal{T}_h) \times \mathcal{P}_k(\mathcal{T}_h)$$

are defined locally on each element $K \in \mathcal{T}_h$ by the following equations

$$\left(\boldsymbol{\Pi}\boldsymbol{\sigma}, \boldsymbol{r}_h\right)_K = \left(\boldsymbol{\sigma}, \boldsymbol{r}_h\right)_K , \qquad \forall \boldsymbol{r}_h \in \boldsymbol{\mathcal{P}}_{k-1}(K), \tag{37a}$$

$$\left(\Pi p, w_h\right)_K = \left(p, w_h\right)_K , \qquad \forall w_h \in \mathcal{P}_{k-1}(K), \tag{37b}$$

$$\langle \boldsymbol{\Pi}\boldsymbol{\sigma} \cdot \boldsymbol{n} + i\omega\tau\Pi p, \mu_h\rangle_{\partial K} = \langle \boldsymbol{\sigma} \cdot \boldsymbol{n} + i\omega\tau p, \mu_h\rangle_{\partial K} , \qquad \forall \mu_h \in \mathcal{R}_k(\partial K), \tag{37c}$$

where $\mathcal{R}_k(\partial K)$ is the space of piecewise polynomials of degree at most k on ∂K

$$\mathcal{R}_k(\partial K) := \prod_{e \in \mathcal{E}(K)} \mathcal{P}_k(e).$$

The HDG projection also satisfies the following *weak commutativity* property

$$\left(\mathrm{div}\left(\boldsymbol{\Pi}\boldsymbol{\sigma}\right), w_h\right)_K + i\omega \left\langle \tau\Pi p, w_h\right\rangle_{\partial K} = \left(\mathrm{div}\left(\boldsymbol{\sigma}\right), w_h\right)_K + i\omega \left\langle \tau p, w_h\right\rangle_{\partial K} , \tag{38}$$

for all $w_h \in \mathcal{P}_k(K)$ on each element $K \in \mathcal{T}_h$, see [DS19, Eq (3.6)]. Notice that denoting the image of $(\boldsymbol{\sigma}, p)$ under $(\boldsymbol{\Pi}, \Pi)$ by $(\boldsymbol{\Pi}\boldsymbol{\sigma}, \Pi p)$ is a slight abuse of notation

as both components depend on $\boldsymbol{\sigma}$ and p. For quantities defined on the skeleton of the mesh, we use the $L^2(\partial\mathcal{T}_h)$-orthogonal projection P_M onto M_h which satisfies

$$\langle P_M p, \mu_h\rangle_{\partial K} = \langle p, \mu_h\rangle_{\partial K}\,, \quad \forall \mu_h \in \mathcal{R}_k(\partial K), \tag{39}$$

on each element $K \in \mathcal{T}_h$. On an element $K \in \mathcal{T}_h$, we also define the *average value* $\{\cdot\}$ by

$$(\{u\}\,, w_h)_K = (u, w_h)_K\,, \quad \forall w_h \in \mathcal{P}_0(K).$$

Furthermore, the error analysis is carried out in the L^2-norm and relies on a Aubin-Nitsche technique. We therefore introduce the following auxiliary problem

$$\boldsymbol{W_0}\boldsymbol{\xi} - \nabla\theta = 0, \qquad \text{in } \mathcal{O}, \tag{40a}$$

$$-\omega^2\rho_0\theta - 2i\omega\boldsymbol{b_0}\cdot\nabla\theta - \operatorname{div}(\boldsymbol{\xi}) = \varepsilon_h^p, \qquad \text{in } \mathcal{O}, \tag{40b}$$

$$\boldsymbol{\xi}\cdot\boldsymbol{n} = 0, \qquad \text{on } \partial\mathcal{O}. \tag{40c}$$

To prove convergence estimates, we assume that this problem is well-posed and satisfies the *elliptic regularity* assumption

$$\|\theta\|_{2,\mathcal{O}} + \|\boldsymbol{\xi}\|_{1,\mathcal{O}} \leqslant C_{\text{reg}}\,\|\varepsilon_h^p\|_{\mathcal{O}}\,. \tag{41}$$

Remark 6.1: As the problem (40a)–(40b)–(40c) can be equivalently written as

$$-\omega^2\rho_0\theta - 2i\omega\boldsymbol{b_0}\cdot\nabla\theta - \operatorname{div}(\boldsymbol{K_0}\nabla\theta) = \varepsilon_h^p,$$

it has the same *coercive + compact* structure as the original problem (3) if the background flow is subsonic (see (5)). This problem is therefore of Fredholm type, and well-posedness is equivalent to uniqueness of the solution. The well-posedness hypothesis thus means that we will consider frequencies ω that are not resonant.

We now state the solvability assumptions under which Theorem 6.1 can be proven.

Assumption 1 (Local solvability)**.** *The local problems are well-posed,* i.e. *when* $\widehat{p_h}$ *is known the local solvers* (8a)–(8b) *uniquely define* $(\boldsymbol{\sigma}_h^K, p_h^K)$ *for all* $K \in \mathcal{T}_h$.

Assumption 2 (Global solvability)**.** *The global problem* (13) *uniquely defines the numerical trace* $\widehat{p_h}$.

The combination of those two assumptions ensures that the HDG method is well-posed. We also add two regularity assumptions.

Assumption 3 (Direct regularity)**.** *The optimal approximation estimates of* Lemma 6.1 *are obtained if the exact solution is regular enough,* i.e. *if* $p|_K \in H^{k+1}(K)$ *and* $\boldsymbol{\sigma}|_K \in \boldsymbol{H}^{k+1}(K)$ *for all* $K \in \mathcal{T}_h$.

Assumption 4 (Aubin-Nitsche regularity)**.** *The elliptic regularity assumption* (41) *for the solution* $(\boldsymbol{\xi}, \theta)$ *of the auxiliary problem* (40a)–(40b)–(40c) *holds.*

Remark 6.2: Notice that the direct regularity assumption addresses the *local* regularity of the exact solution, whereas the Aubin-Nitsche regularity assumptions deals with the *global* regularity of the solution.

It is worth noting that there is a natural set of of sufficient conditions under which Assumption 1, Assumption 2, Assumption 3 and Assumption 4 hold:

(1) the flow is subsonic, *i.e.*

$$\inf_{\mathcal{O}}(\rho_0 c_0 - |\boldsymbol{b_0}|) > 0,$$

(2) ω is not a resonant frequency of the continuous problem,
(3) h is sufficiently small,
(4) the domain $\mathcal{O}$ is either a regular bounded open set, or a convex polyhedron,
(5) $\boldsymbol{W_0}$ and $\boldsymbol{b_0}$ are Lipschitz continuous.

Conditions (1) and (2) ensure that the continuous problem is well-posed. Condition (3) ensures that Assumption 1 holds through Theorem 5.1. Conditions (1), (2), (3) and (4) imply that Assumption 2 holds as it will be detailed in Theorem 7.1. Conditions (4) and (5) ensure that Assumption 4 holds as $\varepsilon_h^p \in W_h(\mathcal{T}_h) \subset L^2(\mathcal{O})$, on this topic see [Gri11, Th. 2.2.2.3 & 4.3.1.4] for the regularity of the domain or [BC13, Sec. 7] for the regularity of the coefficients. Finally the amount of regularity in Assumption 3 is only limited by the regularity of the source term s.

The approximation properties of the HDG projection have intensively been studied in [DS19, Prop. 3.6] and [CGS10, Theorem 2.1]. They are recalled in Lemma 6.1.

Lemma 6.1. *Let $k \geqslant 0$ be the polynomial approximation degree[3], if $p \in H^{\ell+1}(K)$ and $\boldsymbol{\sigma} \in \boldsymbol{H}^{\ell+1}(K)$, then the following inequalities hold*

$$\|\Pi p - p\|_K \lesssim h_K^{m+1} \left(|p|_{m+1,K} + |\mathrm{div}\,(\boldsymbol{\sigma})\,|_{m,K} \right), \tag{42a}$$

$$\|\boldsymbol{\Pi\sigma} - \boldsymbol{\sigma}\|_K \lesssim h_K^{m+1} \left(|\boldsymbol{\sigma}|_{m+1,K} + |p|_{m+1,K} \right), \tag{42b}$$

for any m in $[0, \min(k, \ell)]$.

In order to prove the convergence of the method, it remains to prove the following lemma.

Lemma 6.2. *For $k \geqslant 1$, h sufficiently small and under Assumption 1, Assumption 2, Assumption 3 and Assumption 4, the following estimates hold*

$$\|\varepsilon_h^p\|_{\mathcal{T}_h} := \|p_h - \Pi p\|_{\mathcal{T}_h} = \mathcal{O}(h^{k+2}) \quad ; \quad \|\boldsymbol{\varepsilon}_h^{\boldsymbol{\sigma}}\|_{\mathcal{T}_h} := \|\boldsymbol{\sigma}_h - \boldsymbol{\Pi\sigma}\|_{\mathcal{T}_h} = \mathcal{O}(h^{k+1}).$$

We can now state the main result of this section.

Theorem 6.1 (Convergence of the method)**.** *For $k \geqslant 1$, h sufficiently small, and under Assumption 1, Assumption 2, Assumption 3 and Assumption 4, we have*

$$\|p - p_h\|_{\mathcal{T}_h} = \mathcal{O}(h^{k+1}) \quad ; \quad \|\boldsymbol{\sigma} - \boldsymbol{\sigma}_h\|_{\mathcal{T}_h} = \mathcal{O}(h^{k+1}).$$

Proof:
We split the errors as

$$\begin{cases} p - p_h = \delta_h^p + \varepsilon_h^p \text{ with } \delta_h^p = p - \Pi p, \quad \varepsilon_h^p = \Pi p - p_h, \\ \boldsymbol{\sigma} - \boldsymbol{\sigma}_h = \boldsymbol{\delta}_h^{\boldsymbol{\sigma}} + \boldsymbol{\varepsilon}_h^{\boldsymbol{\sigma}} \text{ with } \boldsymbol{\delta}_h^{\boldsymbol{\sigma}} = \boldsymbol{\sigma} - \boldsymbol{\Pi\sigma}, \quad \boldsymbol{\varepsilon}_h^{\boldsymbol{\sigma}} = \boldsymbol{\Pi\sigma} - \boldsymbol{\sigma}_h, \end{cases} \tag{43}$$

A direct consequence of the Lemma 6.1 is

$$\|\boldsymbol{\delta}_h^{\boldsymbol{\sigma}}\|_{\mathcal{T}_h} + \|\delta_h^p\|_{\mathcal{T}_h} \;=\; O(h^{k+1}), \tag{44}$$

when $\boldsymbol{\sigma}$ and p are smooth enough. The triangular inequality and Lemma 6.2 therefore imply the result and completes the proof of Theorem 6.1.

[3]Even if the case $k = 0$ has no practical interest in the context of HDG method, the approximation inequalities still hold in this case.

To obtain a complete proof of convergence, it only remains to prove LEMMA 6.2.

Proof of Lemma 6.2: The proof of LEMMA 6.2 decomposes itself as follows

(i) we derive an energy-like estimate of the form

$$\|\boldsymbol{\varepsilon}_h^{\boldsymbol{\sigma}}\|_{\mathcal{T}_h} + \|\varepsilon_h^p - \widehat{\varepsilon}_h^p\|_{\partial\mathcal{T}_h} \lesssim \|\varepsilon_h^p\|_{\mathcal{T}_h} + \|\delta_h^p\|_{\mathcal{T}_h} + \|\boldsymbol{\delta}_h^{\boldsymbol{\sigma}}\|_{\mathcal{T}_h}\,, \tag{45a}$$

where $\widehat{\varepsilon}_h^p := P_M p - \widehat{p_h}$ and P_M is the $L^2(\partial\mathcal{T}_h)$-orthogonal onto M_h defined in (39).

(ii) The *Aubin-Nitsche method* allows us to get the estimate

$$\|\varepsilon_h^p\|_{\mathcal{T}_h} \lesssim h\left(\|\boldsymbol{\varepsilon}_h^{\boldsymbol{\sigma}}\|_{\mathcal{T}_h} + \|\delta_h^p\|_{\mathcal{T}_h} + \|\boldsymbol{\delta}_h^{\boldsymbol{\sigma}}\|_{\mathcal{T}_h}\right). \tag{45b}$$

(iii) Those two estimates are combined through a *bootstrapping process* to obtain

$$\|\varepsilon_h^p\|_{\mathcal{T}_h} = \mathcal{O}(h^{k+2}) \quad \text{and} \quad \|\boldsymbol{\varepsilon}_h^{\boldsymbol{\sigma}}\|_{\mathcal{T}_h} = \mathcal{O}(h^{k+1}) \tag{45c}$$

(i) Energy-like estimate. Noticing that the solution $(\boldsymbol{\sigma}, p)$ to the exact problem satisfies the HDG equations (12a)–(12b)–(12c) for a discrete test-function, we can subtract the HDG equations for the numerical solution $(\boldsymbol{\sigma}_h, p_h)$ to the HDG equations for $(\boldsymbol{\sigma}, p)$ to obtain

$$\begin{aligned}(\boldsymbol{W_0}(\boldsymbol{\sigma}-\boldsymbol{\sigma}_h), \boldsymbol{r}_h)_{\mathcal{T}_h} - (p-p_h, \operatorname{div}(\boldsymbol{r}_h))_{\mathcal{T}_h} + 2i\omega\left((p-p_h)\boldsymbol{W_0}\boldsymbol{b_0}, \boldsymbol{r}_h\right)_{\mathcal{T}_h} = \\ - \langle p - \widehat{p_h}, \boldsymbol{r}_h\cdot\boldsymbol{n}\rangle_{\partial\mathcal{T}_h}\,,\end{aligned}$$

$$\begin{aligned}-\omega^2\left(\rho_0(p-p_h), w_h\right)_{\mathcal{T}_h} - \left((\boldsymbol{\sigma}-\boldsymbol{\sigma}_h), \nabla w_h\right)_{\mathcal{T}_h} + \langle(\boldsymbol{\sigma}-\widehat{\boldsymbol{\sigma}_h})\cdot\boldsymbol{n}, w_h\rangle_{\partial\mathcal{T}_h} = 0,\\ \langle(\boldsymbol{\sigma}-\boldsymbol{\sigma}_h)\cdot\boldsymbol{n} - i\omega\tau(p_h-\widehat{p_h}), \mu_h\rangle_{\partial\mathcal{T}_h} = 0.\end{aligned}$$

An integration by parts in the second equation yields

$$-\omega^2\left(\rho_0(p-p_h), w_h\right)_{\mathcal{T}_h} + \left(\operatorname{div}(\boldsymbol{\sigma}-\boldsymbol{\sigma}_h), w_h\right)_{\mathcal{T}_h} + \langle(\boldsymbol{\sigma}_h-\widehat{\boldsymbol{\sigma}_h})\cdot\boldsymbol{n}, w_h\rangle_{\partial\mathcal{T}_h} = 0,$$

and using the definition (9) of $\widehat{\boldsymbol{\sigma}_h}$, we finally obtain

$$-\omega^2\left(\rho_0(p-p_h), w_h\right)_{\mathcal{T}_h} + \left(\operatorname{div}(\boldsymbol{\sigma}-\boldsymbol{\sigma}_h), w_h\right)_{\mathcal{T}_h} - i\omega\langle\tau(p_h-\widehat{p_h}), w_h\rangle_{\partial\mathcal{T}_h} = 0.$$

We then resort to the error decomposition (43)

$$\begin{aligned}(\boldsymbol{W_0}\boldsymbol{\varepsilon}_h^{\boldsymbol{\sigma}}, \boldsymbol{r}_h)_{\mathcal{T}_h} + (\boldsymbol{W_0}\boldsymbol{\delta}_h^{\boldsymbol{\sigma}}, \boldsymbol{r}_h)_{\mathcal{T}_h} - (\varepsilon_h^p, \operatorname{div}(\boldsymbol{r}_h))_{\mathcal{T}_h} - (\delta_h^p, \operatorname{div}(\boldsymbol{r}_h))_{\mathcal{T}_h}\\ + 2i\omega\left(\varepsilon_h^p\boldsymbol{W_0}\boldsymbol{b_0}, \boldsymbol{r}_h\right)_{\mathcal{T}_h} + 2i\omega\left(\delta_h^p\boldsymbol{W_0}\boldsymbol{b_0}, \boldsymbol{r}_h\right)_{\mathcal{T}_h} = -\langle p-\widehat{p_h}, \boldsymbol{r}_h\cdot\boldsymbol{n}\rangle_{\partial\mathcal{T}_h}\,,\end{aligned}$$

$$\begin{aligned}-\omega^2\left(\rho_0\varepsilon_h^p, w_h\right)_{\mathcal{T}_h} - \omega^2\left(\rho_0\delta_h^p, w_h\right)_{\mathcal{T}_h} + \left(\operatorname{div}(\boldsymbol{\varepsilon}_h^{\boldsymbol{\sigma}}), w_h\right)_{\mathcal{T}_h}\\ + \left(\operatorname{div}(\boldsymbol{\delta}_h^{\boldsymbol{\sigma}}), w_h\right)_{\mathcal{T}_h} - i\omega\langle\tau(p_h-\widehat{p_h}), w_h\rangle_{\partial\mathcal{T}_h} = 0,\end{aligned}$$

$$\langle\boldsymbol{\varepsilon}_h^{\boldsymbol{\sigma}}\cdot\boldsymbol{n} + \boldsymbol{\delta}_h^{\boldsymbol{\sigma}}\cdot\boldsymbol{n} - i\omega\tau(p_h-\widehat{p_h}), \mu_h\rangle_{\partial\mathcal{T}_h} = 0.$$

The property of the HDG projection (37a)–(37b)–(37c)–(38) leads to

$$\begin{aligned}-(\delta_h^p, \operatorname{div}(\boldsymbol{r}_h))_{\mathcal{T}_h} = 0, \quad \left(\operatorname{div}(\boldsymbol{\delta}_h^{\boldsymbol{\sigma}}), w_h\right)_{\mathcal{T}_h} = -i\omega\langle\tau\delta_h^p, w_h\rangle_{\partial K}\,,\\ \langle\boldsymbol{\delta}_h^{\boldsymbol{\sigma}}\cdot\boldsymbol{n} + i\omega\tau\delta_h^p, \mu_h\rangle_{\partial\mathcal{T}_h} = 0.\end{aligned}$$

We denote by $\widehat{\varepsilon}_h^p = P_M p - \widehat{p_h}$ and remark that the three previous identities yield

$$\begin{aligned}
-(\delta_h^p, \operatorname{div}(\boldsymbol{r}_h))_{\mathcal{T}_h} + \langle p - \widehat{p_h}, \boldsymbol{r}_h \cdot \boldsymbol{n}\rangle_{\partial\mathcal{T}_h} &= \langle P_M p - \widehat{p_h}, \boldsymbol{r}_h \cdot \boldsymbol{n}\rangle_{\partial\mathcal{T}_h}, \\
&= \langle \widehat{\varepsilon}_h^p, \boldsymbol{r}_h \cdot \boldsymbol{n}\rangle_{\partial\mathcal{T}_h}, \\
(\operatorname{div}(\boldsymbol{\delta}_h^{\boldsymbol{\sigma}}), w_h)_{\mathcal{T}_h} - i\omega\langle\tau(p_h - \widehat{p_h}), w_h\rangle_{\partial\mathcal{T}_h} &= -i\omega\langle\tau(\delta_h^p + p_h - \widehat{p_h}), w_h\rangle_{\partial\mathcal{T}_h} \\
&= -i\omega\langle\tau(\widehat{\varepsilon}_h^p - \varepsilon_h^p), w_h\rangle_{\partial\mathcal{T}_h}, \\
\langle\boldsymbol{\delta}_h^{\boldsymbol{\sigma}}\cdot\boldsymbol{n} - i\omega\tau(p_h - \widehat{p_h}), \mu_h\rangle_{\partial\mathcal{T}_h} &= -i\omega\langle\tau(\delta_h^p + p_h - \widehat{p_h}), \mu_h\rangle_{\partial\mathcal{T}_h} \\
&= -i\omega\langle\tau(\widehat{\varepsilon}_h^p - \varepsilon_h^p), \mu_h\rangle_{\partial\mathcal{T}_h},
\end{aligned}$$

where we used the definition (39) of P_M to obtain

$$\langle\tau\delta_h^p, w_h\rangle_{\partial\mathcal{T}_h} = \langle\tau(p - \Pi p), w_h\rangle_{\partial\mathcal{T}_h} = \langle\tau(P_M p - \Pi p), w_h\rangle_{\partial\mathcal{T}_h},$$

and therefore

$$\begin{aligned}
\langle\tau(\delta_h^p + p_h - \widehat{p_h}), w_h\rangle_{\partial\mathcal{T}_h} &= \langle\tau(P_M p - \widehat{p_h} + p_h - \Pi p), w_h\rangle_{\partial\mathcal{T}_h}, \\
&= \langle\tau(\widehat{\varepsilon}_h^p - \varepsilon_h^p), w_h\rangle_{\partial\mathcal{T}_h}.
\end{aligned}$$

This leads to

$$\begin{aligned}
(\boldsymbol{W_0}\boldsymbol{\varepsilon}_h^{\boldsymbol{\sigma}}, \boldsymbol{r}_h)_{\mathcal{T}_h} - (\varepsilon_h^p, \operatorname{div}(\boldsymbol{r}_h))_{\mathcal{T}_h} + 2i\omega(\varepsilon_h^p\boldsymbol{W_0}\boldsymbol{b_0}, \boldsymbol{r}_h)_{\mathcal{T}_h} + \langle\widehat{\varepsilon}_h^p, \boldsymbol{r}_h\cdot\boldsymbol{n}\rangle_{\partial\mathcal{T}_h} \\
= -(\boldsymbol{W_0}\boldsymbol{\delta}_h^{\boldsymbol{\sigma}}, \boldsymbol{r}_h)_{\mathcal{T}_h} - 2i\omega(\delta_h^p\boldsymbol{W_0}\boldsymbol{b_0}, \boldsymbol{r}_h)_{\mathcal{T}_h},
\end{aligned} \tag{47a}$$

$$-\omega^2(\rho_0\varepsilon_h^p, w_h)_{\mathcal{T}_h} + (\operatorname{div}(\boldsymbol{\varepsilon}_h^{\boldsymbol{\sigma}}), w_h)_{\mathcal{T}_h} + i\omega\langle\tau(\varepsilon_h^p - \widehat{\varepsilon}_h^p), w_h\rangle_{\partial\mathcal{T}_h} = \omega^2(\rho_0\delta_h^p, w_h)_{\mathcal{T}_h}, \tag{47b}$$

$$-\langle\boldsymbol{\varepsilon}_h^{\boldsymbol{\sigma}}\cdot\boldsymbol{n} + i\omega\tau(\varepsilon_h^p - \widehat{\varepsilon}_h^p), \mu_h\rangle_{\partial\mathcal{T}_h} = 0. \tag{47c}$$

Testing (47a)–(47b)–(47c) with $(\boldsymbol{\varepsilon}_h^{\boldsymbol{\sigma}}, \varepsilon_h^p, \widehat{\varepsilon}_h^p)$, conjugating (47a) and summing the resulting equations leads to

$$\begin{aligned}
\|\boldsymbol{\varepsilon}_h^{\boldsymbol{\sigma}}\|_{\boldsymbol{W_0},\mathcal{T}_h}^2 + i\omega\left\|\tau^{1/2}(\varepsilon_h^p - \widehat{\varepsilon}_h^p)\right\|_{\partial\mathcal{T}_h}^2 &= \omega^2\|\varepsilon_h^p\|_{\rho_0,\mathcal{T}_h}^2 + 2i\omega(\boldsymbol{\varepsilon}_h^{\boldsymbol{\sigma}}, \varepsilon_h^p\boldsymbol{W_0}\boldsymbol{b_0})_{\mathcal{T}_h} \\
&\quad - (\boldsymbol{\varepsilon}_h^{\boldsymbol{\sigma}}, \boldsymbol{W_0}\boldsymbol{\delta}_h^{\boldsymbol{\sigma}})_{\mathcal{T}_h} + 2i\omega(\boldsymbol{\varepsilon}_h^{\boldsymbol{\sigma}}, \delta_h^p\boldsymbol{W_0}\boldsymbol{b_0})_{\mathcal{T}_h} + \omega^2(\rho_0\delta_h^p, \varepsilon_h^p)_{\mathcal{T}_h}.
\end{aligned}$$

Notice that the signs of terms multiplied by $i\omega$ in (47a) changed because of the conjugation, *e.g.*

$$\overline{-2i\omega(\delta_h^p\boldsymbol{W_0}\boldsymbol{b_0}, \boldsymbol{\varepsilon}_h^{\boldsymbol{\sigma}})_{\mathcal{T}_h}} = +2i\omega(\boldsymbol{\varepsilon}_h^{\boldsymbol{\sigma}}, \delta_h^p\boldsymbol{W_0}\boldsymbol{b_0})_{\mathcal{T}_h}.$$

Due to the Cauchy-Schwarz inequality, the Young's inequality, the Lemma 5.1-(ii) and the equivalence of norms, we obtain estimate (45a)

$$\|\boldsymbol{\varepsilon}_h^{\boldsymbol{\sigma}}\|_{\mathcal{T}_h}^2 + \|\varepsilon_h^p - \widehat{\varepsilon}_h^p\|_{\partial\mathcal{T}_h}^2 \lesssim \|\varepsilon_h^p\|_{\mathcal{T}_h}^2 + \|\delta_h^p\|_{\mathcal{T}_h}^2 + \|\boldsymbol{\delta}_h^{\boldsymbol{\sigma}}\|_{\mathcal{T}_h}^2.$$

(ii) Aubin-Nitsche estimate. The solution $(\boldsymbol{\xi}, \theta) \in \boldsymbol{H}_{\operatorname{div}}(\mathcal{O}) \times H^1(\mathcal{O})$ to the auxiliary problem (40a)–(40b)–(40c) satisfies

$$\begin{aligned}
(\boldsymbol{W_0}\boldsymbol{\xi}, \boldsymbol{\varepsilon}_h^{\boldsymbol{\sigma}})_{\mathcal{T}_h} + (\theta, \operatorname{div}(\boldsymbol{\varepsilon}_h^{\boldsymbol{\sigma}}))_{\mathcal{T}_h} - \langle\theta, \boldsymbol{\varepsilon}_h^{\boldsymbol{\sigma}}\cdot\boldsymbol{n}\rangle_{\partial\mathcal{T}_h} &= 0, \\
-\omega^2(\rho_0\theta, \varepsilon_h^p)_{\mathcal{T}_h} - 2i\omega(\boldsymbol{b_0}\cdot\nabla\theta, \varepsilon_h^p)_{\mathcal{T}_h} - (\operatorname{div}(\boldsymbol{\xi}), \varepsilon_h^p)_{\mathcal{T}_h} &= (\varepsilon_h^p, \varepsilon_h^p)_{\mathcal{T}_h}, \\
\langle\boldsymbol{\xi}\cdot\boldsymbol{n}, \widehat{\varepsilon}_h^p\rangle_{\partial\mathcal{T}_h} &= 0,
\end{aligned} \tag{48a}$$

Remark 6.3: Notice that the functional framework for (48a) is quite complicated as $\boldsymbol{\xi}\cdot\boldsymbol{n}$ usually cannot be evaluated on the interior edges. However, using the definition of the jump between two elements, we have

$$\langle \boldsymbol{\xi}\cdot\boldsymbol{n}, \widehat{\varepsilon}_h^p\rangle_{\partial\mathcal{T}_h} := \sum_{e\in\mathcal{E}_h^i}\int_e [\![\boldsymbol{\xi}]\!]\overline{\widehat{\varepsilon}_h^p}\mathrm{d}\sigma - \int_{\Gamma_D}(\boldsymbol{\xi}\cdot\boldsymbol{n})\overline{\widehat{\varepsilon}_h^p}\mathrm{d}\sigma.$$

As the right-hand side is well-defined, we can use it to give meaning to the left-hand side.

Introducing the projections $(\boldsymbol{\Pi},\Pi)$ satisying (37a)–(38)–(37c), we remark that

$$(\theta,\operatorname{div}(\boldsymbol{\varepsilon}_h^{\boldsymbol{\sigma}}))_{\mathcal{T}_h} = (\Pi\theta,\operatorname{div}(\boldsymbol{\varepsilon}_h^{\boldsymbol{\sigma}}))_{\mathcal{T}_h}$$

$$(\operatorname{div}(\boldsymbol{\xi}),\varepsilon_h^p)_K = (\operatorname{div}(\boldsymbol{\Pi}\boldsymbol{\xi}),\varepsilon_h^p)_K + i\omega\langle\tau(\Pi\theta-\theta),\varepsilon_h^p\rangle_{\partial K}$$

$$\langle\boldsymbol{\xi}\cdot\boldsymbol{n},\widehat{\varepsilon}_h^p\rangle_{\partial\mathcal{T}_h} = \langle\boldsymbol{\Pi}\boldsymbol{\xi}\cdot\boldsymbol{n},\widehat{\varepsilon}_h^p\rangle_{\partial\mathcal{T}_h} + i\omega\langle\tau(\Pi\theta-\theta),\widehat{\varepsilon}_h^p\rangle_{\partial\mathcal{T}_h}.$$

Since $\boldsymbol{W_0}\boldsymbol{\xi} = \nabla\theta$, it follows

$$(\Pi\theta,\operatorname{div}(\boldsymbol{\varepsilon}_h^{\boldsymbol{\sigma}}))_{\mathcal{T}_h} - \langle\theta,\boldsymbol{\varepsilon}_h^{\boldsymbol{\sigma}}\cdot\boldsymbol{n}\rangle_{\partial\mathcal{T}_h} = -(\boldsymbol{W_0}\boldsymbol{\xi},\boldsymbol{\varepsilon}_h^{\boldsymbol{\sigma}})_{\mathcal{T}_h}, \tag{50a}$$

$$\begin{aligned}-(\operatorname{div}(\boldsymbol{\Pi}\boldsymbol{\xi}),\varepsilon_h^p)_{\mathcal{T}_h} - i\omega\langle\tau(\Pi\theta-\theta),\varepsilon_h^p\rangle_{\partial\mathcal{T}_h}&\\ = \|\varepsilon_h^p\|_{\mathcal{T}_h}^2 + 2i\omega(\boldsymbol{b_0}\cdot\boldsymbol{W_0}\boldsymbol{\xi},\varepsilon_h^p)_{\mathcal{T}_h} + \omega^2(\rho_0\theta,\varepsilon_h^p)_{\mathcal{T}_h},&\end{aligned} \tag{50b}$$

$$\langle\boldsymbol{\Pi}\boldsymbol{\xi}\cdot\boldsymbol{n},\widehat{\varepsilon}_h^p\rangle_{\partial\mathcal{T}_h} + i\omega\langle\tau(\Pi\theta-\theta),\widehat{\varepsilon}_h^p\rangle_{\partial\mathcal{T}_h} = 0. \tag{50c}$$

By conjugating the error equations (47a)–(47b)–(47c) and testing them with $(\boldsymbol{\Pi}\boldsymbol{\xi},\Pi\theta,P_M\theta)$ we obtain

$$\begin{aligned}-(\operatorname{div}(\boldsymbol{\Pi}\boldsymbol{\xi}),\varepsilon_h^p)_{\mathcal{T}_h} + \langle\boldsymbol{\Pi}\boldsymbol{\xi}\cdot\boldsymbol{n},\widehat{\varepsilon}_h^p\rangle_{\partial\mathcal{T}_h}&\\ = -(\boldsymbol{\Pi}\boldsymbol{\xi},\boldsymbol{W_0}(\boldsymbol{\varepsilon}_h^{\boldsymbol{\sigma}}+\boldsymbol{\delta}_h^{\boldsymbol{\sigma}}))_{\mathcal{T}_h} + 2i\omega(\boldsymbol{W_0}\boldsymbol{\Pi}\boldsymbol{\xi},(\varepsilon_h^p+\delta_h^p)\boldsymbol{b_0})_{\mathcal{T}_h},&\end{aligned} \tag{51a}$$

$$(\Pi\theta,\operatorname{div}(\boldsymbol{\varepsilon}_h^{\boldsymbol{\sigma}}))_{\mathcal{T}_h} - i\omega\langle\Pi\theta,\tau(\varepsilon_h^p-\widehat{\varepsilon}_h^p)\rangle_{\partial\mathcal{T}_h} = \omega^2(\Pi\theta,\rho_0(\varepsilon_h^p+\delta_h^p))_{\mathcal{T}_h}, \tag{51b}$$

$$-\langle\theta,\boldsymbol{\varepsilon}_h^{\boldsymbol{\sigma}}\cdot\boldsymbol{n}\rangle_{\partial\mathcal{T}_h} + i\omega\langle\theta,\tau(\varepsilon_h^p-\widehat{\varepsilon}_h^p)\rangle_{\partial\mathcal{T}_h} = 0, \tag{51c}$$

in (51c) we used (39) to replace $P_M\theta$ by θ. Notice that some of the signs changed due to the conjugation, for example in (47b)

$$\overline{i\omega\langle\tau(\varepsilon_h^p-\widehat{\varepsilon}_h^p),\Pi\theta\rangle_{\partial\mathcal{T}_h}} = -i\omega\langle\Pi\theta,\tau(\varepsilon_h^p-\widehat{\varepsilon}_h^p)\rangle_{\partial\mathcal{T}_h}.$$

We notice that the sum of the left-hand sides of (50a)–(50b)–(50c) and (51a)–(51b)–(51c) are equal. We deduce that the right-hand sides are also equal

$$\begin{aligned}&-(\boldsymbol{W_0}\boldsymbol{\xi},\boldsymbol{\varepsilon}_h^{\boldsymbol{\sigma}})_{\mathcal{T}_h} + \|\varepsilon_h^p\|_{\mathcal{T}_h}^2 + 2i\omega(\boldsymbol{b_0}\cdot\boldsymbol{W_0}\boldsymbol{\xi},\varepsilon_h^p)_{\mathcal{T}_h} + \omega^2(\rho_0\theta,\varepsilon_h^p)_{\mathcal{T}_h}\\ &= -(\boldsymbol{\Pi}\boldsymbol{\xi},\boldsymbol{W_0}(\boldsymbol{\varepsilon}_h^{\boldsymbol{\sigma}}+\boldsymbol{\delta}_h^{\boldsymbol{\sigma}}))_{\mathcal{T}_h} + 2i\omega(\boldsymbol{W_0}\boldsymbol{\Pi}\boldsymbol{\xi},(\varepsilon_h^p+\delta_h^p)\boldsymbol{b_0})_{\mathcal{T}_h} + \omega^2(\Pi\theta,\rho_0(\varepsilon_h^p+\delta_h^p))_{\mathcal{T}_h}.\end{aligned}$$

After reorganizing the terms, we obtain

$$\begin{aligned}\|\varepsilon_h^p\|_{\mathcal{T}_h}^2 =& -(\boldsymbol{W_0}(\boldsymbol{\Pi}\boldsymbol{\xi}-\boldsymbol{\xi}),\boldsymbol{\varepsilon}_h^{\boldsymbol{\sigma}}+\boldsymbol{\delta}_h^{\boldsymbol{\sigma}})_{\mathcal{T}_h} - (\boldsymbol{W_0}\boldsymbol{\xi},\boldsymbol{\delta}_h^{\boldsymbol{\sigma}})_{\mathcal{T}_h}\\ &+\omega^2(\rho_0(\Pi\theta-\theta),\varepsilon_h^p+\delta_h^p)_{\mathcal{T}_h} + \omega^2(\rho_0\theta,\delta_h^p)_{\mathcal{T}_h}\\ &+2i\omega(\boldsymbol{b_0}\cdot\boldsymbol{W_0}(\boldsymbol{\Pi}\boldsymbol{\xi}-\boldsymbol{\xi}),\varepsilon_h^p+\delta_h^p)_{\mathcal{T}_h} + 2i\omega(\boldsymbol{b_0}\cdot\boldsymbol{W_0}\boldsymbol{\xi},\delta_h^p)_{\mathcal{T}_h},\end{aligned}$$

since $\nabla\theta = \boldsymbol{W_0\xi}$, see (40a). Introducing the mean value and following the proof of [DS19, Prop. 3.8], we have

$$\begin{aligned}\|\varepsilon_h^p\|_{\mathcal{T}_h}^2 =& -(\boldsymbol{W_0}(\boldsymbol{\Pi\xi}-\boldsymbol{\xi}),\boldsymbol{\varepsilon_h^\sigma}+\boldsymbol{\delta_h^\sigma})_{\mathcal{T}_h} - (\boldsymbol{W_0\xi}-\{\boldsymbol{W_0\xi}\},\boldsymbol{\delta_h^\sigma})_{\mathcal{T}_h}\\ &+\omega^2(\rho_0(\Pi\theta-\theta),\varepsilon_h^p+\delta_h^p)_{\mathcal{T}_h}+\omega^2(\rho_0\theta-\{\rho_0\theta\},\delta_h^p)_{\mathcal{T}_h}\\ &+2i\omega(\boldsymbol{b_0}\cdot\boldsymbol{W_0}(\boldsymbol{\Pi\xi}-\boldsymbol{\xi}),\varepsilon_h^p+\delta_h^p)_{\mathcal{T}_h}+2i\omega(\boldsymbol{b_0}\cdot\boldsymbol{W_0\xi}-\{\boldsymbol{b_0}\cdot\boldsymbol{W_0\xi}\},\delta_h^p)_{\mathcal{T}_h},\end{aligned}$$

since

$$(\{\boldsymbol{W_0\xi}\},\boldsymbol{\delta_h^\sigma})_{\mathcal{T}_h}=0,\quad (\{\rho_0\theta\},\delta_h^p)_{\mathcal{T}_h}=0,\quad (\{\boldsymbol{b_0}\cdot\boldsymbol{W_0\xi}\},\delta_h^p)_{\mathcal{T}_h}=0.$$

Using the Cauchy-Schwarz inequality, we have

$$\begin{aligned}\|\varepsilon_h^p\|_{\mathcal{T}_h}^2 \lesssim& \|\boldsymbol{\Pi\xi}-\boldsymbol{\xi}\|_{\mathcal{T}_h}\left(\|\boldsymbol{\varepsilon_h^\sigma}\|_{\mathcal{T}_h}+\|\boldsymbol{\delta_h^\sigma}\|_{\mathcal{T}_h}\right)+\|\boldsymbol{W_0\xi}-\{\boldsymbol{W_0\xi}\}\|_{\mathcal{T}_h}\|\boldsymbol{\delta_h^\sigma}\|_{\mathcal{T}_h}\\ &+\|\Pi\theta-\theta\|_{\mathcal{T}_h}\left(\|\varepsilon_h^p\|_{\mathcal{T}_h}+\|\delta_h^p\|_{\mathcal{T}_h}\right)+\|\rho_0\theta-\{\rho_0\theta\}\|_{\mathcal{T}_h}\|\delta_h^p\|_{\mathcal{T}_h}\\ &+\|\boldsymbol{\Pi\xi}-\boldsymbol{\xi}\|_{\mathcal{T}_h}\left(\|\varepsilon_h^p\|_{\mathcal{T}_h}+\|\delta_h^p\|_{\mathcal{T}_h}\right)+\|\boldsymbol{b_0}\cdot\boldsymbol{W_0\xi}-\{\boldsymbol{b_0}\cdot\boldsymbol{W_0\xi}\}\|_{\mathcal{T}_h}\|\delta_h^p\|_{\mathcal{T}_h}\end{aligned}$$

Applying Lemma 6.1 with $m=0$[4] to $(\boldsymbol{\xi},\theta)$, since $\|u-\{u\}\|_K \lesssim h_K\|u\|_{1,K}$, and taking the elliptic regularity (41) into account, we obtain

$$\begin{cases}\|\boldsymbol{\Pi\xi}-\boldsymbol{\xi}\|_{\mathcal{T}_h}+\|\Pi\theta-\theta\|_{\mathcal{T}_h}\lesssim h(\|\boldsymbol{\xi}\|_{1,\mathcal{T}_h}+\|\theta\|_{1,\mathcal{T}_h})\lesssim h\|\varepsilon_h^p\|_{\mathcal{T}_h}.\\ \|\boldsymbol{W_0\xi}-\{\boldsymbol{W_0\xi}\}\|_{\mathcal{T}_h}\lesssim h\|\boldsymbol{W_0\xi}\|_{1,\mathcal{T}_h}\lesssim h\|\boldsymbol{\xi}\|_{1,\mathcal{T}_h}\lesssim h\|\varepsilon_h^p\|_{\mathcal{T}_h}\\ \|\rho_0\theta-\{\rho_0\theta\}\|_{\mathcal{T}_h}\lesssim h\|\rho_0\theta\|_{1,\mathcal{T}_h}\lesssim h\|\theta\|_{1,\mathcal{T}_h}\lesssim h\|\varepsilon_h^p\|_{\mathcal{T}_h}\\ \|\boldsymbol{b_0}\cdot\boldsymbol{W_0\xi}-\{\boldsymbol{b_0}\cdot\boldsymbol{W_0\xi}\}\|_{\mathcal{T}_h}\lesssim h\|\boldsymbol{b_0}\cdot\boldsymbol{W_0\xi}\|_{1,\mathcal{T}_h}\lesssim h\|\boldsymbol{\xi}\|_{1,\mathcal{T}_h}\lesssim h\|\varepsilon_h^p\|_{\mathcal{T}_h}.\end{cases}$$

It follows that

$$\|\varepsilon_h^p\|_{\mathcal{T}_h}^2\lesssim h\|\varepsilon_h^p\|_{\mathcal{T}_h}\left(\|\boldsymbol{\varepsilon_h^\sigma}\|_{\mathcal{T}_h}+\|\boldsymbol{\delta_h^\sigma}\|_{\mathcal{T}_h}+\|\varepsilon_h^p\|_{\mathcal{T}_h}+\|\delta_h^p\|_{\mathcal{T}_h}\right).$$

Finally the absorption argument of Lemma 5.1 yields to (45b)

(iii) Bootstrapping process. Using the energy-like estimate (45a) and (44), we have

$$\|\boldsymbol{\varepsilon_h^\sigma}\|_{\mathcal{T}_h}\lesssim\omega\|\varepsilon_h^p\|_{\mathcal{T}_h}+\mathcal{O}(h^{k+1}),$$

Using the dual estimate (45b) and Lemma 5.1, we deduce (45c)

$$\|\boldsymbol{\varepsilon_h^\sigma}\|_{\mathcal{T}_h}=\mathcal{O}(h^{k+1})\text{ and }\|\varepsilon_h^p\|_{\mathcal{T}_h}=\mathcal{O}(h^{k+2}).$$

This completes the proof of Lemma 6.2.

[4]Here, using the highest interpolation inequality of $(\boldsymbol{\Pi},\Pi)$ is not required, and using only the coarsest bound is sufficient to obtain the super-convergence result.

Remark 6.4: The result of LEMMA 6.2 is stronger than what is actually needed to prove THEOREM 6.1 as $\|\varepsilon_h^p\|_{\mathcal{T}_h} = \mathcal{O}(h^{k+1})$ would be sufficient. Actually, we prove that the proposed HDG method achieves *super-convergence*, *ie* taking $p_h \in \mathcal{P}_k$ leads to the following error estimate

$$\|\Pi p - p_h\|_{\mathcal{T}_h} = \mathcal{O}(h^{k+2}).$$

Super-convergence is an attractive property for a numerical scheme, indeed by using a post-processing scheme it is possible to use the solution $(\boldsymbol{\sigma}_h, p_h)$ to construct a new approximation $\widetilde{p_h}$ which converges with order $\mathcal{O}(h^{k+2})$, see [Ste91], [CGS10, Sec. 5] for more details.

7. GLOBAL SOLVABILITY

The analysis that we have carried out in the previous subsection works for any solution $(\boldsymbol{\sigma}_h, p_h, \widehat{p_h})$ of the discrete system (12a)–(12b)–(12c) provided that such solution exists. We already discussed the well-posedness of the local problems in THEOREM 5.1, but we have not yet proved that the global problem (13) for $\widehat{p_h}$ was well-posed.

To do that, we can either directly show the well-posedness of the global problem (13), or we can use the error estimates of THEOREM 6.1 and follow [DS19, End of page 64].

We recall that the convected Helmholtz equation is a problem of Fredholm type. It is therefore uniquely solvable except on a set of *resonant frequencies*. For those frequencies, there exist non-zero solutions to the homogenous equation and unique solvability cannot be guaranteed.

We can now state and prove the main result of this section.

Theorem 7.1 (Global solvability)**.** *Under the assumptions of* THEOREM *5.1 and* THEOREM *6.1 and if ω is not a resonant frequency of the convected Helmholtz equation* (1) *then the global problem is well-posed,* ie *$\widehat{p_h}$ is uniquely defined by* (13)*.*

Proof: First we recall that (12a)–(12b)–(12c), or equivalently (13), is a square system of linear equations, we therefore only need to show the uniqueness of the solution of the homogenous system (when $g_N = g_D = s = 0$).

Assuming that ω is not a resonant frequency of (1), the exact solution is $p = 0$ and $\boldsymbol{\sigma} = \mathbf{0}$, and therefore

$$\|p\|_{s,\mathcal{O}} = 0 \quad \text{and} \quad \|\boldsymbol{\sigma}\|_{t,\mathcal{O}} = 0$$

and

$$\varepsilon_h^p = -p_h \;\; ; \;\; \boldsymbol{\varepsilon}_h^{\boldsymbol{\sigma}} = -\boldsymbol{\sigma}_h \;\; ; \;\; \widehat{\varepsilon}_h^p = -\widehat{p_h}.$$

The estimates from the previous section are

$$\|\varepsilon_h^p\|_{\mathcal{T}_h} \lesssim \|\delta_h^p\|_{\mathcal{T}_h} + \|\boldsymbol{\delta}_h^{\boldsymbol{\sigma}}\|_{\mathcal{T}_h}, \quad \|\boldsymbol{\varepsilon}_h^{\boldsymbol{\sigma}}\|_{\mathcal{T}_h} \lesssim \|\delta_h^p\|_{\mathcal{T}_h} + \|\boldsymbol{\delta}_h^{\boldsymbol{\sigma}}\|_{\mathcal{T}_h}.$$

Going back to (42a)–(42b) we have $\delta_h^p = 0$ and $\boldsymbol{\delta}_h^{\boldsymbol{\sigma}} = 0$. This leads to $p_h \equiv 0$ and $\boldsymbol{\sigma}_h \equiv \mathbf{0}$ since

$$\|p_h\|_{\mathcal{T}_h} = \|\varepsilon_h^p\|_{\mathcal{T}_h} \lesssim 0, \quad \|\boldsymbol{\sigma}_h\|_{\mathcal{T}_h} = \|\boldsymbol{\varepsilon}_h^{\boldsymbol{\sigma}}\|_{\mathcal{T}_h} \lesssim 0,.$$

For all $K \in \mathcal{T}_h$, we can now write that $\widehat{p_h} \equiv 0$. taking into account (8a)

$$\langle \widehat{p_h}, \boldsymbol{r}_h \cdot \boldsymbol{n} \rangle_{\partial K} = 0, \quad \forall \boldsymbol{r}_h \in \boldsymbol{V}_h(K),$$

■

8. Numerical experiments

In this subsection, we will present some numerical experiments to illustrate our theoretical results. Details regarding the implementation of the method in the open-source software `hawen` [Fau21] and performance assessments on realistic problems will be the subject of a forthcoming paper. As most of the estimates obtained in our analysis involve projection errors of the form

$$\|p_h - \Pi p\|_{\mathcal{T}_h} \quad \text{or} \quad \|\boldsymbol{\sigma}_h - \boldsymbol{\Pi}\boldsymbol{\sigma}\|_{\mathcal{T}_h}, \tag{52}$$

we will therefore provide numerical error involving those projection terms, instead of the usual errors

$$\|p_h - p\|_{\mathcal{T}_h} \quad \text{or} \quad \|\boldsymbol{\sigma}_h - \boldsymbol{\sigma}\|_{\mathcal{T}_h}. \tag{53}$$

In particular, the errors involving the projections (52) will allow us to see the *super-convergence* proven in Theorem 6.1, whereas the errors measured by (53) are not of the same order of convergence. Those projections will be computed by locally solving the system (37a)–(37b)–(37c) on each element of the mesh. The integrals in the right-hand side are evaluated using a 91-point Gauss-Lobatto quadrature rule and the resulting linear system is solved using `lapack`. For the purpose of comparing numerical simulations on different meshes, we introduce the *relative* L^2*-errors*

$$\mathcal{E}_q = \frac{\|q_h - \Pi q\|_{\mathcal{T}_h}}{\|\Pi q\|_{\mathcal{T}_h}}, \quad \text{for } q \in \{p, \sigma_x, \sigma_y\}.$$

This quantity is plotted against k/h, which is proportional to the number of degrees of freedom per wavelength. We would like to point out that all the plots in the next sections will use a log-log scale.

8.1. Geometric settings and analytic solution.

As depicted on Figure 5 we consider a uniform directional flow $\boldsymbol{v_0} = Mc_0\boldsymbol{e}_x$, where M is the *Mach number*.

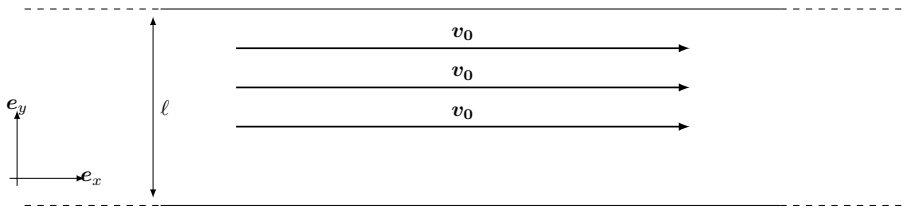

Figure 5. Sketch of the geometric configuration

Unless stated otherwise, we will always use the following parameters for the convergence tests

$$\mathcal{O} = (0,2) \times (0,1) \quad ; \quad \rho_0, c_0 \equiv 1 \quad ; \quad \omega = 5.55\pi,$$

and the choice of M will be specified for each numerical experiment.

Analytic solution: The duct modes are a family of analytic solutions of (1) in a waveguide, see [BBL03]. They are given by

$$p_n^{\pm}(x,y) = e^{i\beta_n^{\pm}x}\varphi_n(y)$$

where

$$n < N_0 : \qquad \beta_n^{\pm} = \frac{-\kappa M \pm \sqrt{\kappa^2 - \frac{n^2\pi^2}{\ell^2}(1-M^2)}}{1-M^2}$$

$$n > N_0 : \qquad \beta_n^{\pm} = \frac{-\kappa M \pm i\sqrt{\frac{n^2\pi^2}{\ell^2}(1-M^2) - \kappa^2}}{1-M^2}$$

with

$$\kappa = \frac{\omega}{c_0} \quad \text{and} \quad M = \frac{v_0}{c_0}$$

$$N_0 = \left\lfloor \frac{\kappa\ell}{\pi\sqrt{1-M^2}} \right\rfloor$$

and

$$\varphi_0(y) := \sqrt{\ell^{-1}}$$
$$\varphi_n(y) := \sqrt{2\ell^{-1}}\cos\left(\frac{n\pi y}{\ell}\right), \quad n \in \mathbb{N}^*$$

The choice of n will be specified for each numerical experiment.

8.2. **Numerical experiment with a low Mach number.** We then move to a flow with a low Mach number. In this case we have used the following parameters

$$n = 3, \quad \text{and} \quad M = 0.2.$$

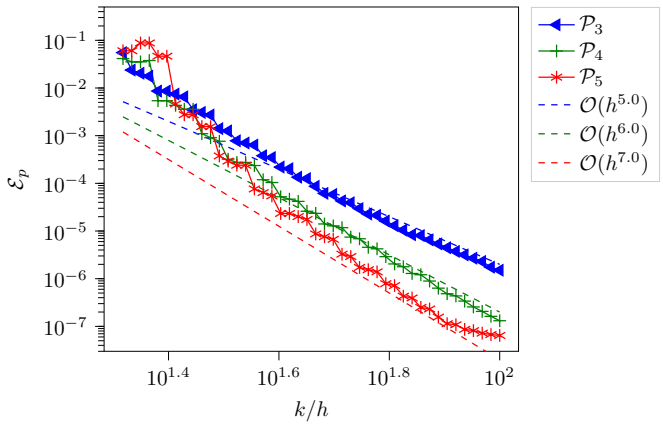

FIGURE 6. Low Mach convergence history for the volumetric unknown p_h

The convergence history for the volumetric unknown p_h is displayed on FIGURE 6. We can see that the method achieves a convergence rate of $k+2$ as expected and actually is super-convergent. The convergence history for the total flux $\boldsymbol{\sigma}_h$ is depicted on FIGURE 7. Once again, the method achieves the expected optimal

convergence rate of $k+1$. When the penalization parameter is badly chosen, the convergence properties of the method may be affected, as illustrated in [Rou21, Sec. 3.6.3].

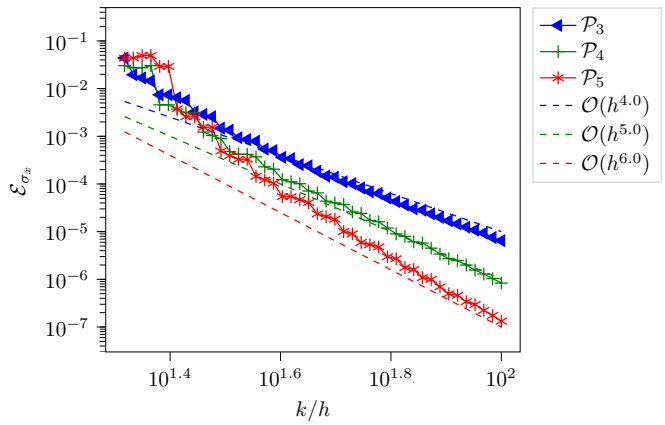

FIGURE 7. Low Mach convergence history for the first component of $\boldsymbol{\sigma}$

8.3. **Numerical experiment with a large Mach number.** Finally we also considered a flow with a large March number. In this case, we used the following parameters

$$n = 3, \quad \text{and} \quad M = 0.8.$$

As the simulations of acoustic wave propagation in flows with large Mach numbers is known to be more challenging, we expect to see worse performances than in the previous subsection.

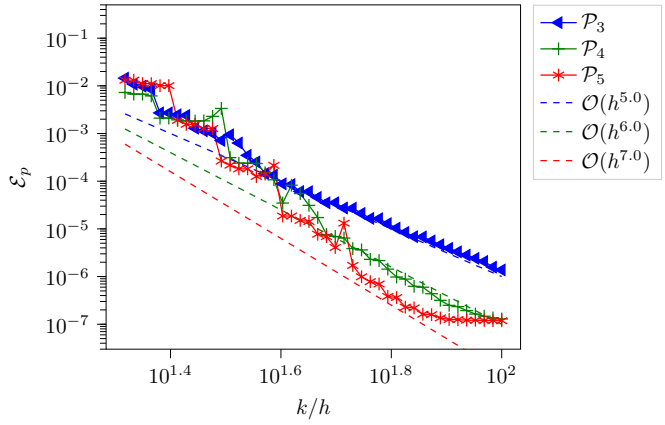

FIGURE 8. Large Mach convergence history for the volumetric unknown p_h

The convergence history for the volumetric unknowns p and $\boldsymbol{\sigma}$ are depicted in FIGURE 8 and FIGURE 9. We can see that the method still has a convergence rate

of $k+2$ for p and $k+1$. The super-convergence of the method is achieved for large Mach numbers for interpolation degree 3 and 4. However the asymptotic regime does not seem totally established for the method with $k=5$. In this case, it seems reasonable to use the HDG method with interpolation degree limited to 3 or 4, as we are not guaranteed to obtain a better accuracy for the additional cost of the method with interpolation degree 5. Furthermore, if a post-processing scheme is used the HDG method with interpolation degree 4 has a convergence rate of 6, which should be sufficient for most applications. This lack of convergence can be explained by the anisotropy of the medium. For large Mach numbers, the solution is rapidly oscillating in some directions. This behavior is difficult to capture with uniform interpolation. In this case, using lower order polynomial interpolation on smaller elements seems to give more accurate results.

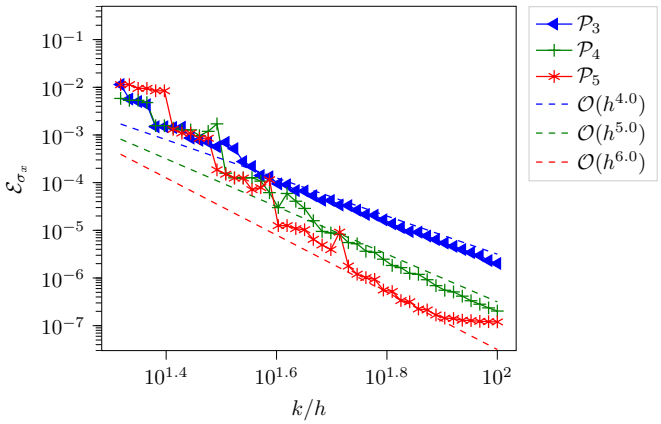

FIGURE 9. Large Mach convergence history for the first component of $\boldsymbol{\sigma}$

CONCLUSION

In this paper we have constructed and analyzed an upwind HDG method for the convected Helmholtz equation. This work was deeply influenced by the important contributions of Francisco-Javier Sayas. We refer to the renct special issue [GHM22] of *Computer Methods in Applied Mathematics* that was dedicated to his memory. Our method is based on the total-flux formulation, where the vectorial unknown encompasses both diffusive and convective effects. For this formulation, we were able to compute a physically informed value of the penalization parameter therefore making the corresponding HDG method easy-to-use, as there is no arbitrary choice of parameter to make.

For this method, detailed theoretical results on well-posedness convergence are provided. These properties are illustrated by numerical experiments that are consistent with the super-convergence phenomenon.

As the HDG method of this paper is super-convergent, it is possible to devise a post-processing scheme to locally enhance the convergence rate of the method. This will be the subject of a future work.

It is also worth noting that the convected Helmholtz equation can be solved by using a diffusive flux formulation. Then. the vectorial unknown only takes diffusive phenomena into account. In the near future, we aim at studying the HDG method that has been proposed in [Rou21] and compare its efficiency with the method we propose herein.

Acknowledgement: An open-source implementation of those three methods in the `hawen` solver ([Fau21]) will be released soon. The authors would like to thank its first developer Florian Faucher for his help with the numerical implementation. The authors would like to thank the anonymous referees for their relevant comments that have helped them to improve this paper.

Experiments presented in this paper were carried out using the PlaFRIM experimental testbed, supported by Inria, CNRS (LABRI and IMB), Université de Bordeaux, Bordeaux INP and Conseil Régional d'Aquitaine (see https://www.plafrim.fr).

Nathan Rouxelin acknowledges financial support from e2s-UPPA (see https://e2s-uppa.eu) and from Maison Normande des Sciences du Numérique (see https://www.criann.fr/mnsn/).

References

[ALA13] Natalia C. B. Arruda, Abimael F. D. Loula, and Regina C. Almeida. Locally discontinuous but globally continuous Galerkin methods for elliptic problems. *Computer Methods in Applied Mechanics and Engineering*, 255:104–120, March 2013. Cited on page 7.

[BBF+17] Helene Barucq, Abderrahmane Bendali, M'Barek Fares, Vanessa Mattesi, and Sebastien Tordeux. A symmetric Trefftz-DG formulation based on a local boundary element method for the solution of the Helmholtz equation. *Journal of Computational Physics*, 330:1069–1092, 2017. Cited on page 2.

[BBL03] Eliane Bécache, Anne-Sophie Bonnet-Ben Dhia, and Guillaume Legendre. Perfectly matched layers for the convected Helmholtz equation. Technical report, 2003. Cited on page 29.

[BC13] Lucio Boccardo and Gisella Croce. *Elliptic Partial Differential Equations*. De Gruyter, Berlin, Boston, 2013. Cited on page 22.

[BCDL15] Marie Bonnasse-Gahot, Henri Calandra, Julien Diaz, and Stéphane Lanteri. Hybridizable Discontinuous Galerkin method for the simulation of the propagation of the elastic wave equations in the frequency domain. Research Report RR-8990, INRIA Bordeaux ; INRIA Sophia Antipolis - Méditerranée, June 2015. Cited on page 2.

[BDE21] Erik Burman, Guillaume Delay, and Alexandre Ern. A hybridized high-order method for unique continuation subject to the Helmholtz equation. *SIAM Journal on Numerical Analysis*, 59(5):2368–2392, 2021. Cited on page 2.

[BDMP21] Hélène Barucq, Julien Diaz, Rose-Cloé Meyer, and Ha Pham. Implementation of hybridizable discontinuous Galerkin method for time-harmonic anisotropic poroelasticity in two dimensions. *International Journal for Numerical Methods in Engineering*, 122(12):3015–3043, 2021. Cited on page 2.

[CC12] Yanlai Chen and Bernardo Cockburn. Analysis of variable-degree HDG methods for convection–diffusion equations. Part I: General nonconforming meshes. *IMA Journal of Numerical Analysis*, 32(4):1267–1293, October 2012. Cited on page 2.

[CC14] Yanlai Chen and Bernardo Cockburn. Analysis of variable-degree HDG methods for convection-diffusion equations. Part II: Semimatching nonconforming meshes. *Mathematics of Computation*, 83(285):87–111, January 2014. Cited on page 2.

[CDG+09] Bernardo Cockburn, Bo Dong, Johnny Guzmán, Marco Restelli, and Riccardo Sacco. A Hybridizable Discontinuous Galerkin Method for Steady-State Convection-Diffusion-Reaction Problems. *SIAM Journal on Scientific Computing*, 31(5):3827–3846, January 2009. Cited on page 2.

[CDPE16] Bernardo Cockburn, Daniele A. Di Pietro, and Alexandre Ern. Bridging the hybrid high-order and hybridizable discontinuous Galerkin methods. *ESAIM: Mathematical Modelling and Numerical Analysis*, 50(3):635–650, May 2016. Cited on page 2.

[CFN19] Théophile Chaumont-Frelet and Serge Nicaise. Wavenumber explicit convergence analysis for finite element discretizations of general wave propagation problems. *IMA Journal of Numerical Analysis*, 40(2):1503–1543, 05 2019. Cited on page 17.

[CGL09] Bernardo Cockburn, Jayadeep Gopalakrishnan, and Raytcho Lazarov. Unified Hybridization of Discontinuous Galerkin, Mixed, and Continuous Galerkin Methods for Second Order Elliptic Problems. *SIAM J. Numer. Anal*, 47:1319–1365, August 2009. Cited on pages 2 and 11.

[CGS10] Bernardo Cockburn, Jayadeep Gopalakrishnan, and Francisco-Javier Sayas. A projection-based error analysis of HDG methods. *Mathematics of Computation*, 79(271):1351–1367, March 2010. Cited on pages 2, 10, 22, and 27.

[Chr04] Jorgen Christensen-Dalsgaard. *Lecture Notes on Stellar Oscillations*. 2004. Cited on page 1.

[CLOS20] Liliana Camargo, Bibiana López-Rodríguez, Mauricio Osorio, and Manuel Solano. An HDG method for Maxwell's equations in heterogeneous media. *Computer Methods in Applied Mechanics and Engineering*, 368:113178, August 2020. Cited on page 2.

[Coc14] Bernardo Cockburn. Static Condensation, Hybridization, and the Devising of the HDG Methods. *springerprofessional.de*, 2014. Cited on page 2.

[CQS18] Huangxin Chen, Weifeng Qiu, and Ke Shi. A priori and computable a posteriori error estimates for an HDG method for the coercive Maxwell equations. *Computer Methods in Applied Mechanics and Engineering*, 333:287–310, May 2018. Cited on page 2.

[CQSS17] Huangxin Chen, Weifeng Qiu, Ke Shi, and Manuel Solano. A Superconvergent HDG Method for the Maxwell Equations. *Journal of Scientific Computing*, 70(3):1010–1029, March 2017. Cited on page 2.

[CS98] Bernardo Cockburn and Chi-Wang Shu. The Local Discontinuous Galerkin Method for Time-Dependent Convection-Diffusion Systems. *SIAM Journal on Numerical Analysis*, 35(6):2440–2463, 1998. Cited on page 12.

[CS13] Bernardo Cockburn and Ke Shi. Superconvergent HDG methods for linear elasticity with weakly symmetric stresses | IMA Journal of Numerical Analysis | Oxford Academic. *IMA Journal of Numerical Analysis*, 2013. Cited on page 2.

[DS19] Shukai Du and Francisco-Javier Sayas. *An Invitation to the Theory of the Hybridizable Discontinuous Galerkin Method: Projections, Estimates, Tools*. SpringerBriefs in Mathematics. Springer International Publishing, Cham, 2019. Cited on pages 2, 20, 22, 26, and 27.

[EG04] Alexandre Ern and Jean-Luc Guermond. *Theory and Practice of Finite Elements*. Applied Mathematical Sciences. Springer-Verlag, New York, 2004. Cited on pages 5 and 19.

[Fau21] Florian Faucher. hawen: time-harmonic wave modeling and inversion using hybridizable discontinuous galerkin discretization. *Journal of Open Source Software*, 6(57):2699, 2021. Cited on pages 1, 28, and 32.

[FCS15] Guosheng Fu, Bernardo Cockburn, and Henryk Stolarski. Analysis of an HDG method for linear elasticity. *International Journal for Numerical Methods in Engineering*, 102(3-4):551–575, 2015. Cited on page 2.

[FLd14] Cristiane O. Faria, Abimael F. D. Loula, and Antônio J. B. dos Santos. Primal stabilized hybrid and DG finite element methods for the linear elasticity problem. *Computers & Mathematics with Applications*, 68(4):486–507, August 2014. Cited on page 7.

[FS20] Florian Faucher and Otmar Scherzer. Adjoint-state method for Hybridizable Discontinuous Galerkin discretization, application to the inverse acoustic wave problem. *Computer Methods in Applied Mechanics and Engineering*, 372:113406, December 2020. Cited on pages 1 and 2.

[GBD+17] Laurent Gizon, Hélène Barucq, Marc Durufle, Chris Hanson, Michael Leguèbe, Aaron Birch, Juliette Chabassier, Damien Fournier, Thorsten Hohage, and Emanuele Papini. Computational helioseismology in the frequency domain: Acoustic waves in axisymmetric solar models with flows. *Astronomy and Astrophysics - A&A*, 600:A35, 2017. Cited on page 1.

[GHM22] Gabriel N. Gatica, Norbert Heuer, and Salim Meddahi. Numerical analysis & no regrets. special issue dedicated to the memory of francisco javier sayas. *Computational Methods in Applied Mathematics*, 22(4):751–755, 2022. Cited on page 31.

[GM11] Roland Griesmaier and Peter Monk. Error Analysis for a Hybridizable Discontinuous Galerkin Method for the Helmholtz Equation. *Journal of Scientific Computing*, 49(3):291–310, December 2011. Cited on page 2.

[Gri11] Pierre Grisvard. *Elliptic Problems in Nonsmooth Domains*. Society for Industrial and Applied Mathematics, 2011. Cited on page 22.

[GSV18] Jay Gopalakrishnan, Manuel Solano, and Felipe Vargas. Dispersion Analysis of HDG Methods. *Journal of Scientific Computing*, 77(3):1703–1735, December 2018. Cited on page 2.

[HPS17] Allan Hungria, Daniele Prada, and Francisco-Javier Sayas. HDG methods for elastodynamics. *Computers & Mathematics with Applications*, 74(11):2671–2690, December 2017. Cited on page 2.

[HW08] Jan S. Hesthaven and Tim Warburton. *Nodal Discontinuous Galerkin Methods: Algorithms, Analysis, and Applications*. Texts in Applied Mathematics. Springer-Verlag, New York, 2008. Cited on pages 12 and 13.

[Jac21] Pierre Jacquet. *Time-Domain Full Waveform Inversion using advanced Discontinuous Galerkin method*. PhD thesis, Université de Pau et des Pays de l'Adour, 2021. Cited on page 2.

[KSC12] Robert J. Kirby, Spencer J. Sherwin, and Bernardo Cockburn. To CG or to HDG: A Comparative Study. *Journal of Scientific Computing*, 51(1):183–212, April 2012. Cited on pages 2, 5, and 6.

[LeV02] Randall J. LeVeque. *Finite Volume Methods for Hyperbolic Problems*. Cambridge Texts in Applied Mathematics. Cambridge University Press, 2002. Cited on page 12.

[NPRC15] Ngoc-Cuong Nguyen, Jaime Peraire, Fernando Reitich, and Bernardo Cockburn. A phase-based hybridizable discontinuous Galerkin method for the numerical solution of the Helmholtz equation. *Journal of Computational Physics*, 290:318–335, June 2015. Cited on page 2.

[PE12] Daniele Antonio Di Pietro and Alexandre Ern. *Mathematical Aspects of Discontinuous Galerkin Methods*. Mathématiques et Applications. Springer-Verlag, Berlin Heidelberg, 2012. Cited on pages 10, 13, and 18.

[Pie90] Allan Pierce. Wave equation for sound in fluids with unsteady inhomogeneous flow. *The Journal of the Acoustical Society of America*, 87(6):2292–2299, June 1990. Cited on page 3.

[Rou21] Nathan Rouxelin. *Condensed Mixed Numerical Methods for Convected Acoustics. Applications in Helioseismology*. PhD thesis, Université de Pau et des Pays de l'Adour, 2021. Cited on pages 11, 30, and 32.

[SM50] Jack Sherman and Winifried Morrison. Adjustment of an Inverse Matrix Corresponding to a Change in One Element of a Given Matrix. *Annals of Mathematical Statistics*, 21(1):124–127, March 1950. Cited on page 4.

[Ste91] Rolf Stenberg. Postprocessing schemes for some mixed finite elements. *ESAIM: Mathematical Modelling and Numerical Analysis*, 25(1):151–167, 1991. Cited on page 27.

[YMKS16] Sergey Yakovlev, David Moxey, Robert M. Kirby, and Spencer J. Sherwin. To CG or to HDG: A Comparative Study in 3D. *Journal of Scientific Computing*, 67(1):192–220, April 2016. Cited on page 2.

MAKUTU, Inria, TotalEnergies, Université de Pau et des Pays de l'Adour, France
Email address: helene.barucq@inria.fr

MAKUTU, Inria, TotalEnergies, Université de Pau et des Pays de l'Adour, France
Current address: Laboratoire de Mathématiques de l'INSA, INSA de Rouen–Normandie, Normandie Université, France
Email address: nathan.rouxelin@inria.fr

MAKUTU, Inria, TotalEnergies, Université de Pau et des Pays de l'Adour, France
Email address: sebastien.tordeux@inria.fr